‘Aortic remodeling after endovascular aneurysm repair’

Deborah Zagers
Master’s thesis Technical Medicine
Date of Graduation: 13 September 2021

Graduation committee
Chairman: Prof.dr. R.H. Geelkerken
Medical supervisor: Prof.dr. R.H. Geelkerken
Technical supervisors: J.A. Simmering, MSc & Prof.dr.ir. C.H. Slump
Process supervisor: Drs. R.M. Krol
Independent assessor: Dr. M. Heijblom

In collaboration with University Medical Center Groningen:
Dr. R.C.L. Schuurmann & Prof.dr. J.P.P.M. de Vries

MST umcg

UNIVERSITY OF TWENTE.

Summary

An endovascular aneurysm repair (EVAR) is currently preferred as treatment for an infrarenal abdominal aortic aneurysm (AAA). Despite good short-term results, major drawbacks of the EVAR treatment are the long-term complications. Recent research has shown that examining the aortic remodeling after EVAR can give new insights into the underlying causes of these complications. Aortic remodeling can be expressed in static measurements such as the postoperative change in aortic diameters, lengths, angles and curvatures measured on computed tomography angiography (CTA) scans, but also as the postoperative change in aortic motion measured on electrocardiogram (ECG)-gated CTA scans. The first chapters of this thesis focused on the aortic remodeling base on static measurements while the last chapter focused on aortic remodeling based on motions.

Anaconda vs Endurant – intra- and interobserver variability

In this thesis measurements on CTA-scans of two types of EVAR endografts were compared: the Anaconda and Endurant. The Endurant cohort had been measured previously by a different observer. In order to compare the Anaconda cohort with the Endurant cohort, an intra- and inter observer variability was determined.

Out of 106 Endurant patients measured by observer 1, 20 patients were measured by observer 2. Measurements were performed twice to obtain the intra observer variability. The pre-EVAR CTA and the first post-EVAR CTA scan was included for each patient. Per scan an aortic and an iliac center luminal line (CLL) was drawn which served as base for curvature calculations. Curvature was defined over the following segments: suprarenal aorta, infrarenal aorta, aneurysm, right common iliac artery and left common iliac artery. Moreover, the following dimensional measurements were performed: baseline diameter, end of neck diameter, neck length, maximal aneurysm diameter alpha angle and beta angle.

Moderate intra- as well as interobserver agreement was observed for aortic curvature measurements. The limitations of this study prohibit a fair statement about the reliability of curvature as a whole. Nonetheless, this observer study does imply that the CLLs, the basis for curvature calculations, should be constructed with great care, which requires an adequate training. Excellent intra- and interobserver agreement was found for the dimensional measurements which is in line with the results in previous literature.

Anaconda vs Endurant – Aortic remodeling

Different types of endograft can cause aortic remodeling to more or lesser extent. Therefore, in this study aortic remodeling was assessed of endografts that easily conform to the curvature of the aorta (Anaconda) and relatively stiff endografts (Endurant). These endografts do not only differ in stiffness but also contain different types of proximal sealing and fixation. The initial aim of this thesis was to compare the aortic remodeling of the Anaconda endograft with the de Endurant endograft, based on curvature and aortic neck diameters measured on pre- and postoperative CTA scans. However, the intra- and inter observer study showed moderate agreement between the observers for aortic curvature. Therefore, aortic remodeling was determined based on aortic neck diameters alone.

The CTA scans of 63 Anaconda patients were compared to the CTA scans of 106 Endurant patients. The same measurement protocol as used for the intra and interobserver variability was used. Aortic diameters were measured at 30 mm above the baseline, 15 mm above the baseline, baseline, 5 mm below baseline and 10 mm below baseline.

The diameters of the Anaconda cohort remained stable, while the diameters in the Endurant cohort increased at all levels except at 30 mm above the baseline. These results imply that the Anaconda rings exert less forces on the aortic wall than the Endurant anchor pins with M-shaped design, resulting in less aortic remodeling. Future research should include post-EVAR follow-up scans to remodeling over time. Moreover, future research should include patient outcome to examine relations between the remodeling and the possible complications.

The influence on motion detection of 8 versus 10 phases ECG-gated CT scans

A study within the present research line compares two types of iliac branched devices (IBDs). The patient cohort with the first device was scanned with an ECG-gated CT scan protocol reconstructing 8 cardiac phases, while the patient cohort with the other device was scanned with an ECG-gated CT scan protocol reconstructing 10 cardiac phases. An in vitro experiment was performed to assess to what extent this phase difference can induce a difference in detected motions. Moreover, an explorative patient study was performed to assess the results in clinical setting.

An in-house developed linear actuator device was used to obtain a controlled motion in one direction to assess a series of ECG-gated CT scans of a moving endograft at different virtual heartrates. An aortic pressure profile was used as movement input. All ECG-gated CT scans were reconstructed to 8 and 10 phases cardiac volumes. Specialized algorithms were used to assess the motion amplitudes and pathlengths of the endograft. The methodology was further tested on the clinical data of a patient.

The in vitro experiment of this study did not reveal a clinical significant difference between the motions amplitudes and the pathlengths of the 8 and 10 phased reconstructions. Also, the patient study did not show any difference both reconstructions. A potential limitation of the in vitro experiment could be that the linear actuator was not synchronized with the CT scanner. A computer simulation showed possible outcomes for the pathlengths of 8 and 10 phases reconstructions. The pathlenghts of the 10 phases reconstructions could be, at maximum, 0.56 mm higher than the pathlengths of the 8 phases reconstructions, depending on the starting point of the CT scanner. Therefore, when comparing ECG-gated CTA scans using 8 phases cardiac cycles with 10 phases cardiac cycles, a difference of maximum 0.56 mm could be explained by the difference in phases. A future study using a synchronized set-up should reduce this value.

Table of contents

List of abbreviations

AAA	Abdominal Aortic Aneurysm
BIF	Bifurcation
CFA	Common Femoral Artery
CIA	Common Iliac Artery
CLL	Center Luminal Line
COPD	Chronic Obstructive Pulmonary Disease
CT	Computed Tomography
CTA	Computed Tomography Angiography
CTR	Celia Trunk
DLF	Distal radiopaque endomarker at the end of the Left endograft limb Fabric
DRF	Distal radiopaque endomarker at the end of the Right endograft limb Fabric
ECG	Electrocardiogram
EIA	External Iliac Artery
EIN	End of Infrarenal Neck
EVAR	Endovascular Aneurysm Repair
Fr	French
HRA	Highest Renal Artery
IBD	Iliac Branched Device
ICC	Intraclass Correlation Coefficient
IIA	Internal Iliac Artery
IQR	Inter Quartile Range
LFP	Left Profunda Femoris
LII	Left Internal Iliac artery
LRA	Lowest Renal Artery
mm	Millimeter
MST	Medisch Spectrum Twente
PF	Proximal radiopaque endomarker of the endograft main body Fabric
RFP	Right Profunda Femoris
RII	Right Internal Iliac artery
SD	Standard Deviation
SMA	Superior Mesenteric Artery
UMCG	University Medical Center Groningen

1 Background

1.1 Abdominal Aortic Aneurysm

When the abdominal aorta is dilated to a diameter of about 1.5 times the diameter of a non-dilated aorta (~30mm), it is called an abdominal aortic aneurysm (AAA) (1). In Europe, the prevalence among males aged 65 years and older is 1-2%, while the prevalence among females is significantly lower (0.5%) (2). In addition to the male gender, risk factors for AAA include smoking, age 60 years and older, hypertension, atherosclerosis, obesity, Caucasian race and positive family history (1,3). Most AAAs are asymptomatic and are found coincidentally on medical imaging for other purposes (1). Symptomatic AAAs, expressed as abdominal pain or back pain, have an increased risk of rupture.

Depending on the location of the AAA, an AAA can be classified into different types (See Figure 1-1). The most common type is the infrarenal AAA, which occurs below the aortic neck. The aortic neck is defined as the non-dilated aorta segment distal to the lowest renal artery. A juxtarenal AAA is defined as an aneurysm starting immediately distally from the lowest renal artery. It includes the infrarenal neck, but does not include the renal arteries (4,5). A pararenal AAA includes at least one of the renal arteries but does not extent suprarenal. A suprarenal AAA extends up to the superior mesenteric artery (5). AAAs can extend to the iliac arteries. This thesis mainly focuses on infrarenal AAAs.

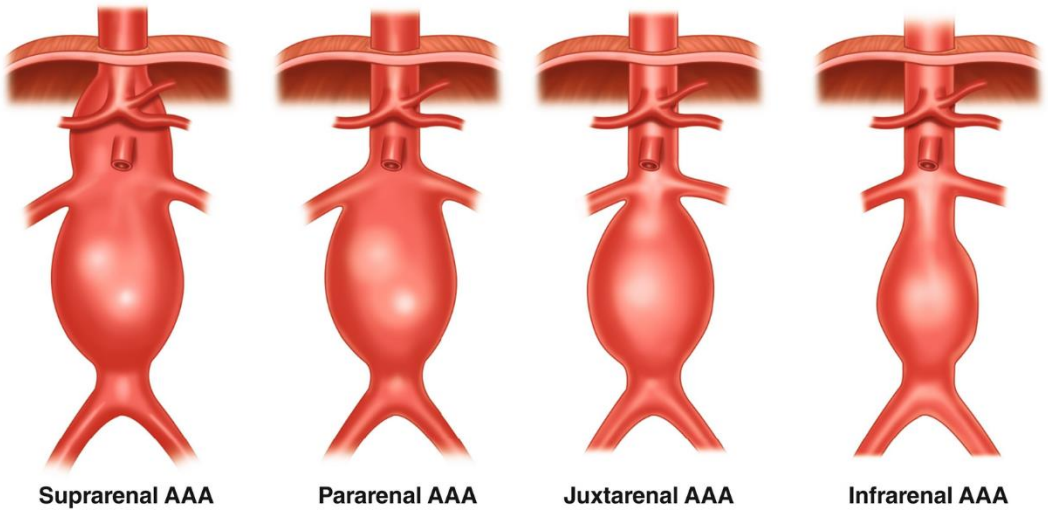

Figure 1-1 Schematic presentation of different types of abdominal aortic aneurysms (6)

An AAA can grow slowly with an average growth of 2.2 mm per year (7). An extensive growth of >5 mm per year increases the risk of rupture (1). Additional risks for aneurysm rupture and/or growth are a symptomatic AAA, persistent smoking, female gender and severe chronic obstructive pulmonary disease (COPD) (3,4). Rupture of an AAA is associated with a mortality rate of 80% (5,8). When an aneurysm reaches a diameter of 55 mm in males or 50 mm in females, the risk of rupture increases to 3-15% (1). Surgical repair has a mortality rate of 0.7-4.0% for males, and 1.8-6.9% for females, open and endovascular treatments combined. Therefore, elective surgery is recommended, when the AAA diameter exceeds the threshold of 55 mm in males and 50 mm in females. Moreover, surgery is recommended when the AAA is symptomatic and/or when the aneurysm grows more than 10 mm per year (5).

1.2 Endovascular Aneurysm Repair

1.2.1 Open vs EVAR

Elective treatment of an AAA can be performed via an open approach or via an Endovascular Aneurysm Repair (EVAR). An open repair is the conventional surgical technique for treating an AAA. It was first performed in the 1950s (9). The procedure is as follows; A median laparotomy through the *linea alba* from the xiphoid to the pubis is needed to approach the AAA (5). The intestines need to be pulled aside carefully. Cross clamping of the abdominal aorta above and below the AAA is required to be able to open the aneurysm sac. Consecutively, the blood cloths inside the aneurysm sac are removed after which a prosthetic graft is anastomosed proximally and distally to the nondilated aortic wall to exclude the aneurysm sac from the blood flow. The aneurysm sac is then placed over the graft and stitched together again. Next, the intestines are released and the abdomen is closed up. This procedure is highly invasive and has a 30-day mortality rate of 3.0% – 4.7% (10,11). The open procedure is therefore not suitable for old or vulnerable patients (5,12). A laparoscopic approach is not a favorable alternative as previous research has shown that it involves more risks than the conventional technique, even with a well-trained surgical team (13).

A less invasive alternative would be the EVAR procedure. It was first performed in 1987 by Volodos et al.(14). Instead of making a large incision in the abdomen, the EVAR method requires only two bilateral small incisions in the groin area to reveal the common femoral arteries (CFAs). Even total percutaneous access is achievable (15). The procedure is executed as follows: guided by fluoroscopy, the endograft is introduced through the CFA using guide wires. After the correct location is determined, the endograft is deployed in the aneurysm and therewith, it excludes the aneurysm from the circulation (5). Radial forces and small hooks at the proximal end of the endograft provide a seal and fixation of the graft (5). Currently, EVAR is preferred in almost 75% of the surgical AAA treatments because of the lower short-term morbidity and mortality (0.7% - 1.5%) compared to open surgery (10,11,16–18). However, this benefit is compensated by the long-term mortality rate of the EVAR procedure. On a long-term base, the mortality rate for the EVAR approach is similar to that of an open repair or even worse, since EVAR is associated with a higher reintervention rate than an open procedure (11,16–20).

1.2.2 Complications

Reinterventions after EVAR procedures are often caused by EVAR-specific complications, such as stent-graft migration, limb occlusion and endoleaks (21). Endoleaks occur in 20-25% of the EVAR patients (22). Endoleaks are defined as the post-EVAR leakage of blood back into the aneurysm sac. There are different causes for endoleaks which result in different endoleak types (See Figure 1-2). In type I endoleaks, blood flows into the aneurysm sac via the proximal (type Ia) or distal (type Ib) fixation zone. During 5-year follow-up the occurrence of type I endoleaks is about 5%. Urgent endovascular reintervention is required at type I endoleaks, as the leakage into the aneurysm sac increases the risk of rupture (21,22). These endoleaks are the main cause of secondary aneurysm ruptures (5). In type II endoleaks, blood leakage into the aneurysm sac is caused by retrograde flow of branch vessels such as the inferior mesenteric artery or the lumbar arteries (23). Type IIa includes one vessel while type IIb includes two or more vessels. These type II endoleaks are the most common endoleaks (20-40%) (5). They can thrombose spontaneously, which is followed by a conservative observational treatment (23). Persistent or recurrent type II endoleaks that result in significant increase in size of the aneurysm sac can be treated by coil embolization of the leaking arteries (5,23). Type III endoleaks include leakage through an endograft caused by a gap between two components (Type IIIa) or a defect in the graft material (Type IIIb). Type III endoleaks occur in 1-3% of the EVAR patients during 5-year follow-up and require immediate reintervention (5). Type IV endoleaks occur in only 1% of the cases. These endoleaks result from blood flow through the pores of the endograft and

are therefore typically resolved postoperative, once the blood clotting has normalized (21,22). Lastly, if the aneurysm sac grows without an identifiable cause, the endoleak is classified as type V, which is also known as endotension. The occurrence of endotension is about 1-5% (24). In case of persistent growth of the aneurysm sac open conversion may be required (25).

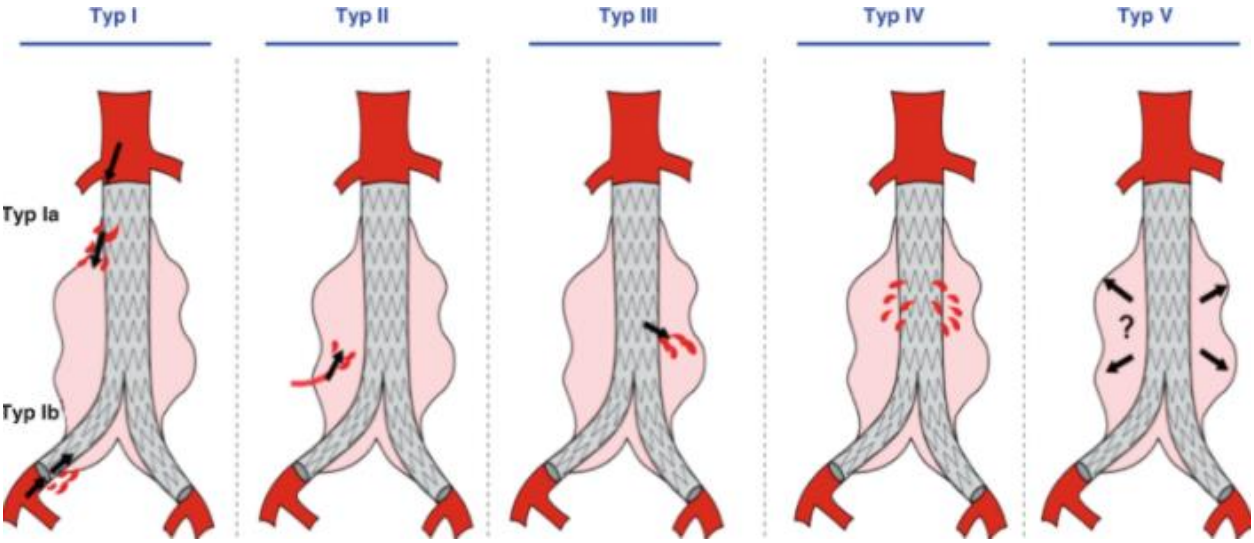

Figure 1-2 Schematic presentation of different types of endoleak (26)

1.2.3 Exclusion Criteria EVAR

EVAR is not an option for patients with an unsuitable anatomy. For example, the infrarenal neck must be long and wide enough, but not too wide, or too angulated, in order to the maintain an adequate proximal landing zone for the graft (27). The same applies to the iliac vessels for a distal fixation. In addition, calcification and thrombus may also cause inadequate sealing and should therefore be avoided in the landing zones (27). The precise cut-off values for the lengths and angles of each segment differ per type of endograft. The details for the two graft-types used in this thesis can be found in section 1.2.4. Unfortunately, patients with unsuitable anatomy for EVAR often have more comorbidities and are therefore not a candidate for open repair as well (27). Off-label use of the endografts is related to worse outcomes (28). It is therefore important to understand the changes occurring in the aorta after placement of an endograft, and how these changes may contribute to possible complications. With this knowledge we can improve endografts and consequently broaden the inclusion criteria to treat patients with more challenging anatomies.

1.2.4 Types Endograft

Several types of endograft have been designed for EVAR procedures by different manufacturers, for example: Excluder (W.L. Gore, Flagstaff, Ariz, USA), Zenith (Cook, Bloomington, Ind, USA), Anaconda (Terumo-Aortic, Inchinnan, Scotland) and Endurant (Medtronic Inc, Minneapolis, USA). This study mainly focuses on the Anaconda and Endurant Endografts, which are further explained in this section.

Anaconda (Terumo-Aortic, Inchinnan, Scotland)

The Anaconda endograft has been on the market since 2005 and is designed for patients with a more angulated and tortuous anatomy with angulations up to 90 degrees (29,30). Other indication details on the Anaconda are shown in Table 1-1. The graft contains a self-expanding flexible body with two saddle-shaped nitinol rings located proximally. These contain four pairs of hooks, with one hook-pair on each peak and valley of the proximal sealing ring. The endograft limbs contain multiple self-expandable rings which maintain the flexibility of the endograft and prevent the graft from kinking as shown in figure Figure 1-3(29,30). Furthermore, the fixation and sealing properties prove their value as low rates of migration and type 1 endoleaks were reported for this endograft (31). However, the main drawback of the Anaconda endograft is the relatively high rate of limb occlusion which is at the upper threshold of the acceptable range (32). One study showed that this relatively high limb occlusion rate might be related to the infolding of graft fabric over time, also called the concertina effect (33).

Figure 1-3 Anaconda Endograft (left) and Endurant endograft (right) (34) (35)

Endurant (Medtronic Inc, Minneapolis, USA)

The Endurant endograft has been on the market since 2008 and is designed to overcome several anatomic limitations usually seen in EVAR procedures (34). The Endurant allows for inclusion of patients with a shorter aortic neck and patients with severe neck angulation up to 75 degrees for the infrarenal neck (See Table 1-1) (35). The Endurant has a sinusoidal M-shape design, preventing the infolding of the fabric when bending the graft, while maintaining radial forces, see Figure 1-3 (36). The suprarenal anchor pins provide secure proximal fixation. Although durable clinical results are observed, one study including 156 Endurant patients showed a reintervention rate of 22.1%, with a median clinical follow-up of 5.9 years (37).

Table 1-1 Anatomical inclusion criteria Anaconda and Endurant

Structure	Anaconda	Endurant
Aortic neck diameter, mm	17.5-31	19-32
Aortic neck length, mm	≥15	≥10 or ≥15
Aortic neck angulation	≤90°	≤60° or ≤75°
Distal fixation length, mm	≥20	≥15
Iliac diameter, mm	8.5-21	8-25
Access artery diameter*, Fr	>20-22	>18-20

Source: Anaconda: instructions for use (38)*, Endurant: Instructions for use* (39)*.*

**Based on outer diameter sheath for delivering the main body*

1.2.5 Current Research on EVAR

Although the results of various newly designed endografts seem promising, long-term complications still remain a problem. The geometry of the AAA is likely to change after insertion of an endograft. Detailed information about these changes could help explain the causes of the long-term complications. Previous studies have already linked some aortic characteristics to EVAR related complications. Recent research showed that aortic curvature seems to have a promising predictive value of treatment outcome (33,40–43). This curvature methodology proved to be more accurate for measuring the aortic neck angulation than the golden standard (41). The total curvature as measured over the aortic neck, aneurysm sac and terminal aorta was found to be an accurate predictor of intraoperative type Ia endoleaks (42). Furthermore, the maximum curvature over the aneurysm sac was found to be a strong predictor of late type Ia endoleak and endograft migration (40). Moreover, curvature in endograft limbs can be used to assess the changes in geometry over time, leading to new predictors of limb occlusion (33,43). Curvature has not been implemented in clinical practice yet. Nonetheless, it is beneficial to investigate the aortic remodeling after EVAR based on curvature, by looking into the postoperative aortic curvature changes. This is because when a relatively stiff endograft is placed in an aorta with large curvature, it may straighten the aorta, which induces forces on the aortic wall. These tensions may result in displacement of the endograft and consequently stent graft migration and possibly ineffective sealing resulting in type Ia endoleaks (44). Curvature can be determined over the whole aortic trajectory and therefore provide insight in if and where this aortic straightening occurs.

To determine the curvature a center luminal line (CLL) is used. Curvature is defined as the inverse of the radius of the spherical shape. This sphere is fitted on the curve at each coordinate along the CLL (See Figure 1-5). The three dimensional curvature can be calculated using the formula of extrinsic linear curvature κ as shown in equation 1.1.

$$\kappa = \frac{\sqrt{(z''y'-y''z')^2 + (x''z'-z''x')^2 + (y''x'-x''y')^2}}{(x'^2+y'^2+z'^2)^{3/2}} \quad [1.1]$$

Where x, y, and z are the Cartesian coordinates for points along a CLL, $'$ is the first derivative and $''$ is the second derivative.

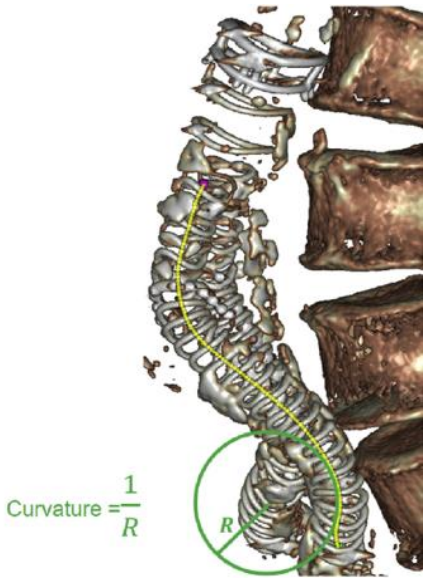

Figure 1-4 Example of curvature approach (33)

Other current research focuses on analyzing dynamic changes of the aorta after insertion of an endograft. The aorta is under constant influence of the pulsatile blood flow. The pressure changes of the pulsatile blood flow may challenge the fixation and sealing of the endograft. High preoperative pulsality in the aneurysm neck has been associated with postoperative stent graft migration already (35). Moreover, examining the change dynamic behavior in the aorta caused by endografts can help improve the future generation endograft designs and predict endograft failure in individual patients (45,46).
The aortic motion patterns can be analyzed using retrospective electrocardiogram (ECG)-gated computed tomography angiography (CTA) scans. This technique provides a three dimensional CTA volume at different phases of the cardiac cycle. ECG-gated CTA scans use the patients ECG signal as trigger to create a CT scan of a full cardiac cycle. The raw data is reconstructed into a predefined number of CT volumes corresponding to phases of the cardiac cycle. Klein et al.(47,48) and Koenrades et al.(49) developed an image registration and segmentation algorithm that allows quantitatively and qualitatively analysis of in vivo motions of the endograft. A current study within the present research line, uses this algorithm to quantitatively characterize and compare the motion and geometry of two types of iliac branched devices (IBDs). The study data was obtained from different hospitals using a different number of cardiac phases to reconstruct the CT volumes. As a result, the patient cohort that was treated with the first device was scanned with an ECG-gated CT scan protocol that reconstructed 8 cardiac phases, while the patient cohort that was treated with the other device was scanned with an ECG-gated CT scan protocol that reconstructed 10 cardiac phases. It is not known to what extent such a difference in phases can lead to a difference in detected motion patterns. Therefore, a study must be conducted to determine the difference between 8 phases reconstructions and 10 phases reconstructions of ECG-gated CTA scans.

1.3 Thesis objectives

This thesis is divided into two main studies divided into 3 chapters. Since relatively little is known about the aortic remodeling after EVAR, the first main study of thesis aims to describe the aortic remodeling based on aortic diameters and curvatures. Aortic remodeling of endografts that can easily conform to the curvature of the aorta, like the Anaconda was compared to aortic remodeling of relatively stiff endografts, like the Endurant. The second main study in this thesis aims to determine the difference between 8 and 10 phases reconstructions of ECG-gated CTA scans, in order to compare motions of IBDs that were scanned with protocol using 8 and 10 phases reconstructions.

Chapter 2: Intra- and interobserver variability on abdominal aortic aneurysm geometries in computer tomography scans.
The measurements that were used to assess the aortic remodeling of the Endurant and Anaconda patients were performed by two observers. Therefore, these measurements were subject to interobserver variability. The aim of this study was to determine the intra- and interobserver variability on the aortic geometries in pre- and post-EVAR CTA scans when measured by two non-experienced observers.

Chapter 3: Aortic remodeling after EVAR: Anaconda vs Endurant
In this study, the aortic remodeling of the Anaconda endograft was compared with the aortic remodeling of the Endurant endograft. Due to moderate observer agreement on curvature, remodeling based on curvature could not be assessed. Therefore, aortic modeling was examined only for the postoperative change in supra, juxta and infrarenal diameters.

Chapter 4: The influence on cardiac-pulsatility-induced motion detection calculation electrocardiographically-gated computed tomography angiography scans reconstructed into 8 or 10 cardiac phases

This study focused on dynamic remodeling by comparing two different types of ECG-gated scanning protocols. This research is part of a study within the present research line that compares two types of iliac branched devices (IBDs). The patient cohort that was treated with the first device was scanned with an electrocardiogram (ECG)-gated computed tomography (CT) scan protocol that reconstructed 8 cardiac phases, while the patient cohort that was treated with the other device was scanned with an ECG-gated CT scan protocol that reconstructed 10 cardiac phases. In order to compare the motion patterns and dynamic geometrical properties of the IBDs, the extent to which the phase difference induces differences in calculated motion should be determined, which was the aim of this thesis. An in vitro-experiment was designed to determine the differences.

2 Intra- and interobserver variability on abdominal aortic aneurysm geometries in computer tomography scans

2.1 Introduction

Endovascular aneurysm repair (EVAR) is currently preferred as treatment for an infrarenal abdominal aortic aneurysm (AAA) (10,11,16–18). It prevents the AAA from rupturing by excluding it from the blood flow. Despite good short and mid-term results, major drawbacks of the EVAR treatment are the long-term complications, which include stent-graft migration, limb occlusion and the occurrence of endoleaks (21). Research has been conducted in order to explore the cause of these complications, with the aim of improving the EVAR treatment. Studies have linked some anatomical characteristics to complications, such as a hostile infrarenal neck (50). Specifically, recent research shows that curvature of the infrarenal aortic neck has a promising predictive value for intraoperative as well as late type 1a endoleaks and migration (40,42). Moreover, one study showed that curvature can be used to assess the aortic remodeling after EVAR (51). They found that the aorta straightens after implantation of an endograft which can affect the risk at late type 1a endoleak and migration. However, this research only focused on the influence of the curvature at the supra- and infrarenal neck and did not include more flexible endografts which are able to conform to severe curvature, like the Anaconda endograft. Therefore, this thesis aimed to compare the aortic remodeling based on curvature over the whole trajectory from the suprarenal aorta up to and including the common iliac arteries. Moreover, the influence of the endograft type on the aortic remodeling was examined by including patients with a relatively stiff endograft (Endurant) and an endograft that easily conforms to the curvature of the aorta (Anaconda). Furthermore, aortic remodeling is not only expressed by a change in curvature, but by a combination of several geometric properties. In this thesis, remodeling was defined as the postoperative change in aortic diameters and curvatures measured on computed tomography angiography (CTA) scans.

The measurements of the Endurant and the Anaconda patients were performed by different observers, making the measurements subject to interobserver variability. The intra- and interobserver variability in AAA dimension measurements on CTA scans has been examined before (52–54). Yet, there is no information available of the intra- and interobserver variability on the aortic curvature. Moreover, curvatures in previous studies were assessed by experienced observers, while the measurements in this study were performed by students (41,55). Thus, the aim of this study was to determine the intra- and interobserver variability on the aortic geometries in pre- and post-EVAR CTA scans when measured by two less experienced observers.

2.2 Methods

2.2.1 Study Design

In this retrospective study, the interobserver variability was determined between two Technical Medicine Master's students. Observer 1 performed the measurements on CTA scans of 106 patients who were treated with an Endurant endograft (Endurant II(s) , Medtronic Inc., Santa Rosa, CA, USA), according to a predefined standardized protocol. Patients were selected from a database of EVAR patients between January 2014 and December 2017 in St. Antonius Hospital (AZN), Nieuwegein, The Netherlands or in the Royal Oldham Hospital (ROH), Oldham, United Kingdom. Inclusion and exclusion have been described previously (56). Out of these 106 patients, 20 patients were measured by observer 2. The pre-EVAR CTA and the first post-EVAR CTA scan were included for each patient. To compensate for the learning curve of both observers, the first and the last 10 patients measured by observer 1 were selected. Moreover, 5 test-scans were selected from another database to use as training material to familiarize observer 2 with

3mensio. In order to obtain an intraobserver variability as well, all 20 patients were measured twice by observer 2. These second measurements were performed at least three weeks after the first measurements. Additionally, the measurement order of patients was randomized to avoid recall bias.

2.2.2 Image acquisition

The scan protocol has been described previously (56). The scan parameters included: tube potentials 120 kV, tube current 180 mAs, collimation 128x0.625 mm, pitch factor 0.9. The slice thicknesses were 1.0 mm (interquartile range 1.0, 2.0) and 2.0 mm (interquartile range 1.0, 2.0) for the pre- and post-EVAR CTA scans, respectively. CT scans were acquired in the arterial phase, using bolus triggering with a threshold of 100 Hounsfield units.

2.2.3 Measurement protocol

The measurement protocol is included in Appendix A. A summary of the protocol is given below. Figure 2-1 illustrates the measurement workflow.

Center luminal line (CLL)

The measurements were conducted with the 3mensio workstation (3mensio Vascular 10.1, Pie Medical Imaging BV, Maastricht, The Netherlands). The aortoiliac trajectory was segmented by selecting the aortic lumen. Missing arteries were added manually. For each scan aorta CLL and an iliac CLL was created, see Figure 2-2. The aorta CLL was obtained by placing a marker above the celiac trunk (~5 cm above the origin of the lowest renal artery) and a second marker below the aortic bifurcation. As was not possible to place the second marker outside the lumen, the marker was placed in either one of the common iliac arteries and corrected after the CLL was automatically drawn between the two markers by the software. The second marker was then moved from the iliac artery to center between both iliac arteries and the CLL points above were manually adjusted in the extension of the aortic bifurcation as shown in Figure 2-2A. The aorta CLL in the post-EVAR scans cannot be positioned in the center of the lumen as the limbs of the endograft were bifurcated in the infrarenal aorta. Therefore, the aorta CLL in post-EVAR scans was placed in the middle between the endograft limbs, see Figure 2-2B. The iliac CLL was created by placing a marker above the celiac trunk, above the native aorta bifurcation (pre-EVAR) or graft bifurcation (post-EVAR) and just below the origin of the profunda femoris artery, see Figure 2-2C and Figure 2-2D.

The CLL pathway points were manually repositioned or added to ensure equal distance to the vessel wall in all planes, as shown in Figure 2-3. In case of an asymmetrical aorta, the expected position of the endograft should be taken into account. For example, in case of a protrusion, the CLL should be in the middle of the expected aorta and not moved to the center of the protrusion, to avoid high curvatures in a straight aorta, as depicted in Figure 2-4. The presence of infrarenal calcification or thrombus was defined according to the Chaikof criteria (57): Absent; calcification or thrombus <25% of circumference; mild; calcification or thrombus 25% to 50% of circumference; moderate; calcification or thrombus ≥50% of circumference. In the presence of mild thrombus and/or calcification it was assumed that the endograft will adapt to the walls of the vessel. The thrombus and/or calcification is therefore determined as luminal area. In the presence of moderate or severe thrombus and/or calcification, the remaining luminal area

should be used to draw the CLL, as it is assumed that the endograft cannot adapt to the vessel wall in those cases.

Figure 2-1 Workflow of measurements *CLL, Center luminal line*

Reference markers

After creating the CLL, reference markers were placed as shown in Figure 2-5. The coordinates of these markers were used for analysis of the dimension measurements and curvature segments. In the aortic CLL, a marker was placed at the caudal edge of the lowest renal artery (LRA) origin, indicated as baseline. If an accessory renal artery was present, the post-EVAR scan was examined to see if the endograft placement was targeted at the accessory renal artery. If so, the caudal edge of the accessory renal artery was defined as baseline. Furthermore, markers were placed at the caudal edges of the origins of the highest renal artery (HRA), superior mesenteric artery (SMA) and celiac trunk (CTR). Moreover, a marker was placed at the end of the infrarenal neck (EIN), defined as a diameter increase of 10% with regard to the baseline.

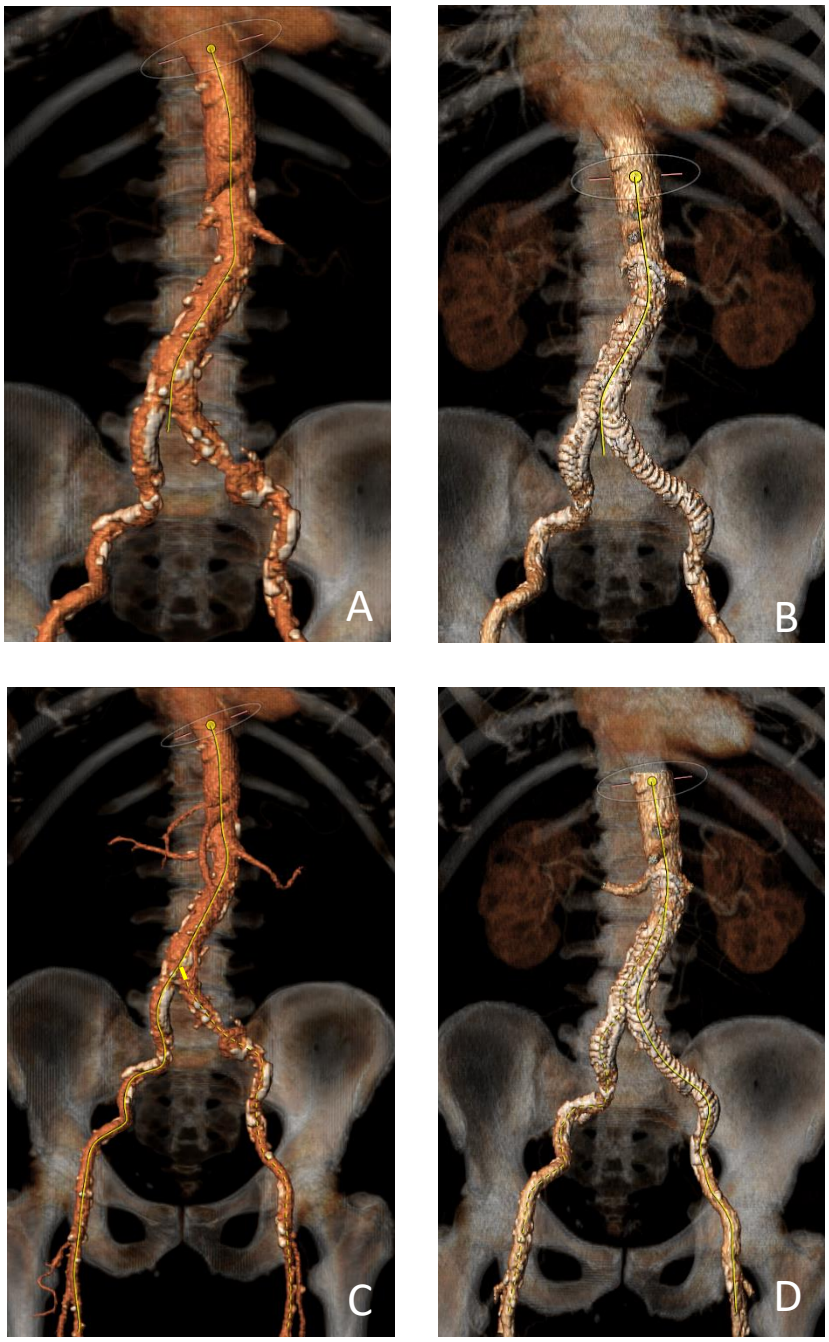

Figure 2-2 Types of center luminal lines (CLL) *A, Preoperative aorta CLL drawn from above the celiac trunk to below the aorta bifurcation; B, postoperative aorta CLL drawn from above the celiac trunk to below the native aorta bifurcation through the middle of the endograft limbs; C, preoperative iliac CLLs drawn from above the celiac trunk to below the origin of the profunda femoris artery; D, postoperative iliac CLLs drawn from above the celiac trunk to below the origin of the profunda femoris artery, bifurcating above the endograft main body flow splitter.*

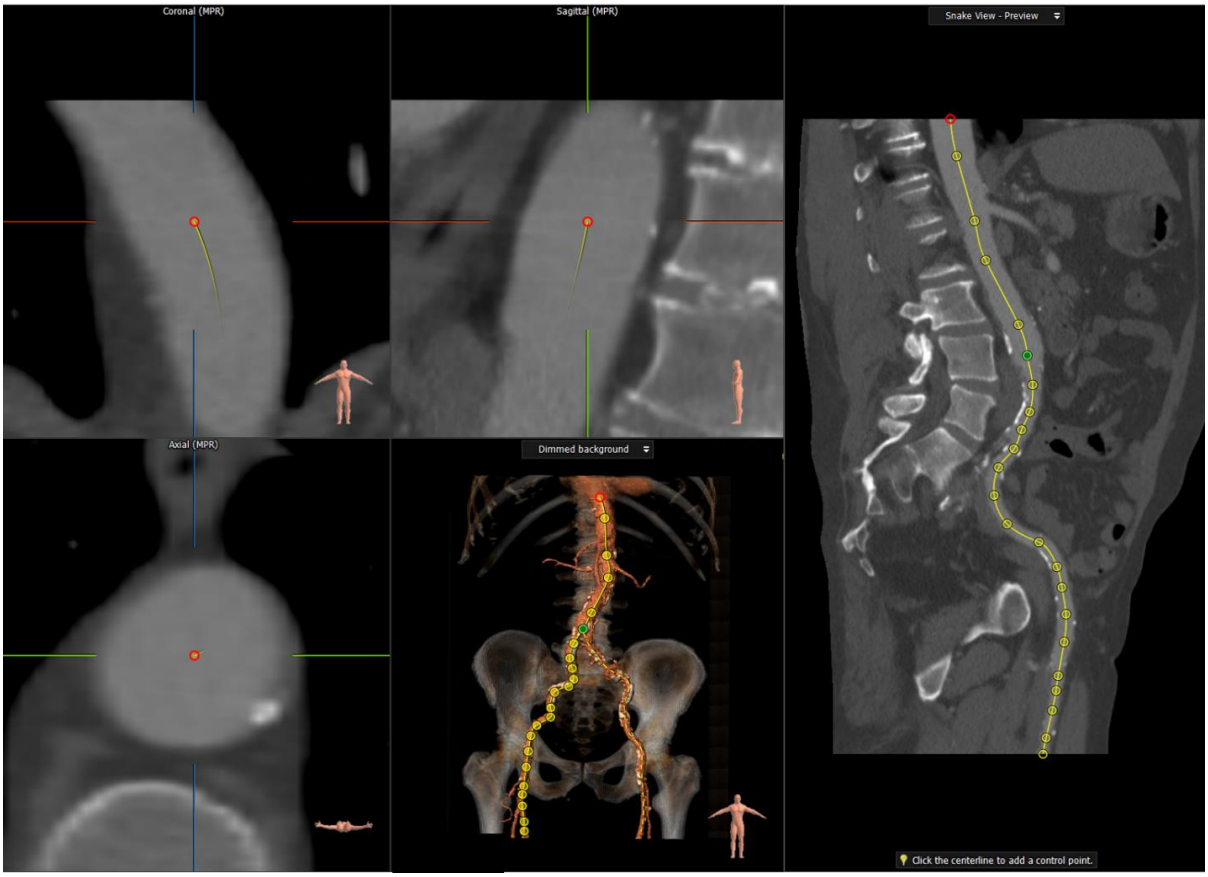

Figure 2-3 Example of the creation of a iliac center luminal line (CLL). *The CLL pathway points were manually repositioned or added to ensure equal distances to the vessel wall in all planes.*

Figure 2-4 Example of center luminal line in case of an aortic protrusion.

Finally, a marker was placed at the aortic bifurcation (BIF). In the iliac CLL, markers were placed at the aortic bifurcation, at the cranial edges of the origins of the right and left internal iliac artery (RII and LII) and the cranial edges of the right and left profunda femoris artery (RFP and LFP). In the post-EVAR scans a reference marker was placed in the aortic CLL at the most proximal radiopaque endomarker of the endograft main body fabric (PF) and in the iliac CLL at the most distal radiopaque endomarker at the end of the endograft limb fabric right and left (DRF and DLF), in addition to the pre-EVAR reference markers.

Diameters, neck length and angulations

Diameters were measured in the plane orthogonal to the CLL from adventitia to adventitia at the baseline, end of aortic neck and maximum aneurysm. At each level the diameter was defined as the average value of the minimum and maximum diameter. In presence of moderate calcification or thrombus, as defined in the CLL section above, the inner diameter was measured for the baseline and end of neck diameter. The maximum aneurysm diameter was measured at the plane perpendicular to the CLL with the largest diameter of the aneurysm sac. This plane was determined by visual inspection. The infrarenal neck length was measured as the length of the CLL between the baseline and the end of the aortic neck, as defined in the reference markers section above. Furthermore, the angulation of the aortic neck was measured with an alpha angle, defined as the maximum angle between the luminal axis of the suprarenal aorta and the infrarenal neck, and a beta angle, defined as the maximum angle between the luminal axis of the infrarenal neck and the aneurysmal sac(58). The angles were measured in degrees.

Curvatures

The coordinates of the CLLs and reference markers were used to calculate curvatures by numerical computation, using the mathematical definition of extrinsic linear curvature given in equation 1.1. For more details on the curvature definitions, see section 1.3. The CLL and marker coordinates were exported from 3mensio, and processed using specialized Matlab software (The MathWorks, Natick Massachusetts, USA), which has been used previously for AAA segment curvature calculations (33,42). The software includes an algorithm that computes the maximum and average curvature for each of the following predefined segments, see also Figure 2-5:

1. Suprarenal aorta. From 50 mm above the baseline to the baseline.
2. Infrarenal aorta. From the baseline to the end of the aortic neck.
3. Aneurysm. From the end of the infrarenal neck to the aortic bifurcation.
4. Right common iliac artery. From the aortic bifurcation to the cranial edge of the origin of the internal iliac artery.
5. Left common iliac artery. From the aortic bifurcation to the cranial edge of the origin of the internal iliac artery.

The suprarenal aorta, infrarenal aorta and aneurysm segments were derived from the aortic CLL while, the common iliac artery segments were calculated from the iliac CLL.

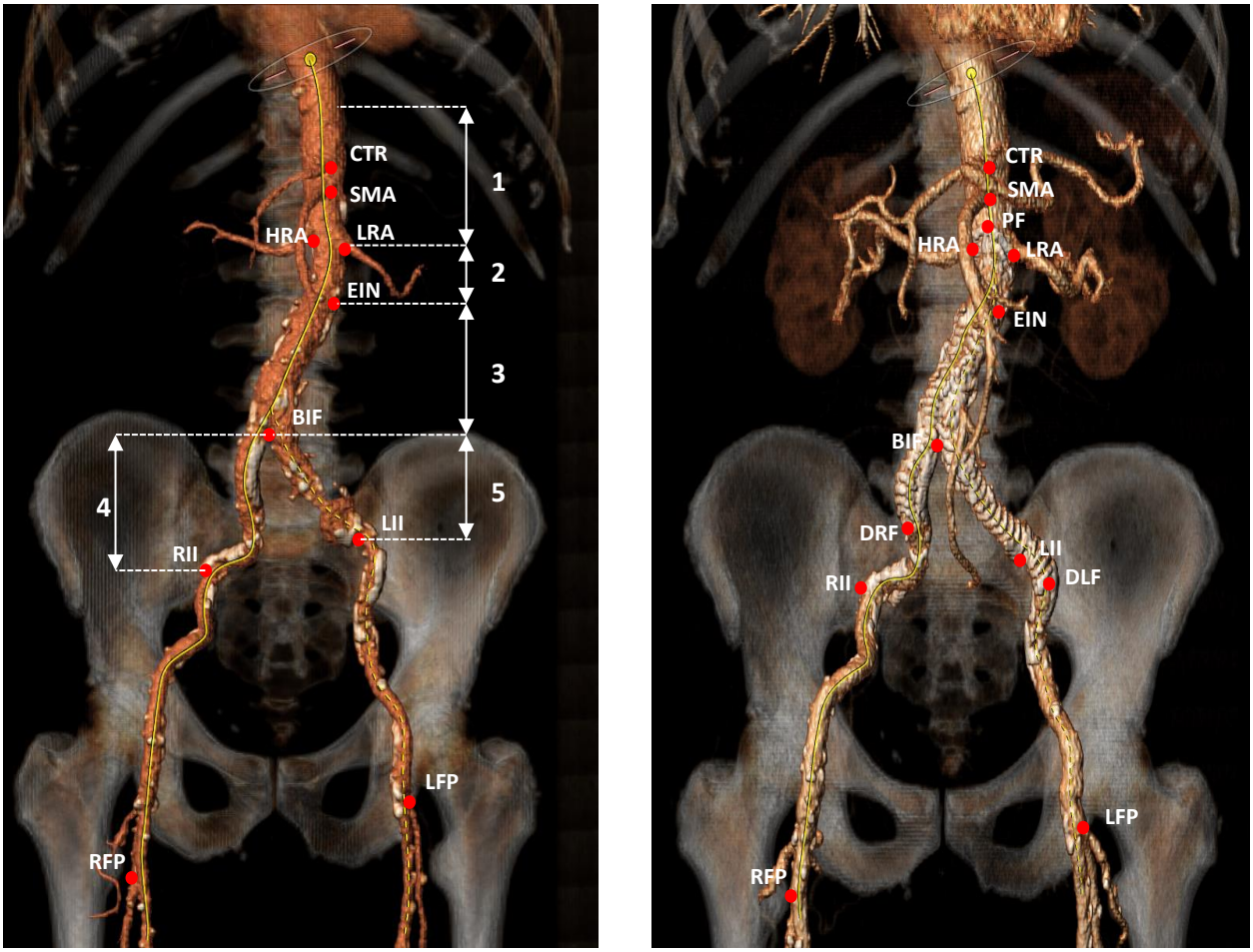

Figure 2-5 Example of marker placement and curvature segments pre-EVAR (left) and post-EVAR (right) *Aorta center luminal line (CLL) markers and iliac CLL markers are presented in one image. Curvature was defined for the following segments: 1, suprarenal; 2 ,infrarenal; 3, aneurysm; 4, right common iliac artery; 5, left common iliac artery. CTR, celiac trunk; BIF, Bifurcation; DRF, distal end of endograft fabric right; DLF, distal end of endograft fabric left; HRA, highest renal artery; LRA, lowest renal artery, LFP; left femoral profunda; LII, left internal iliac artery; EIN, end of infrarenal neck; PF, proximal end of endograft fabric; RFP, right femoral profunda; RII, right internal iliac artery; SMA, superior mesenteric artery;*

2.2.4 Statistical Analysis

The intraclass correlation coefficient (ICC) was used to quantify the degree of agreement between the measurements for the intra- and interobserver variability. The ICCs were reported as ICC [interquartile range, IQR] and an ICC of >0.75 was considered as sufficient (59). Geometric measurements and curvatures were reported as median [IQR] All statistical analyses were performed using IBM SPSS Statistics for Windows (version 25.0; IBM Corporation, Armonk, NY, USA).

2.3 Results

2.3.1 Baseline patient characteristics

Table 2-1 shows the baseline patient characteristics. Of two patients the curvature could not be compared because the curvatures determined by observer 1 were not retrievable.

Table 2-1 Baseline patient characteristics

	n=20
Age (years)	75 [70.5 82.5]
Male Gender	18 (90%)
Hypertension	5 (25%)
Diabetes	3 (15%)
Ischemia	2 (10%)
COPD	6 (30%)

Data shown as median [interquartile range] or number (%).
COPD, Chronic obstructive pulmonary disease;

2.3.2 Interobserver variability

Diameters, neck length and angulations

Excellent agreement was observed for all structures (ICC 0.83 - 0.99) of the 20 included patients, see Table 2-2. The absolute differences between observer 1 and observer 2 of the diameters and lengths are <1.0 mm.

Table 2-2 Interobserver variability geometric measurements

Structure	Observer 1	Observer 2	Difference O1-O2	ICC	P-value
Baseline diameter (mm)	24.1 [22.2 25.7]	23.0 [21.3 24.2]	0.9 [0.2 1.8]	0.91 [0.33 0.97]	<.001
End neck diameter (mm)	26.7 [23.9 28.4]	25.2 [23.5 27.0]	0.5 [0.2 2.3]	0.83 [0.58 0.93]	<.001
Maximum aneurysm diameter (mm)	59.8 [56.4 65.3]	58.9 [55.8 65.0]	0.6 [-0.2 1.8]	0.99 [0.96 1.00]	<.001
Neck length (mm)	16.5 [10.0 33.0]	17.1 [10.5 32.6]	0.0 [-1.5 3.0]	0.99 [0.98 1.00]	<.001
Alpha angle (°)	32.0 [22.0 50.5]	33.0 [24.0 54.0]	2.0 [-8.0 5.5]	0.94 [0.84 0.97]	<.001
Beta angle (°)	62.5 [45.0 71.5]	60.5 [44.5 69.0]	4.5 [-2.0 8.5]	0.89 [0.73 0.96]	<.001

Measurements and measurement differences are presented as median [Q1 Q3]. ICC is presented with 95% confidence interval.
ICC, intraclass correlation coefficient; O1, observer 1; O2, observer 2.

Curvatures

Table 2-3 shows that that preoperative ICCs of the maximum suprarenal curvature, average and maximum aneurysm curvature, average right iliac curvature and maximum left iliac curvature were all below the threshold value of 0.75. Three of these ICCs crossed the threshold value of 0.75 postoperatively, namely the average suprarenal curvature, of which the ICC went from 0.84 preoperatively to 0.66 postoperatively, the maximum aneurysm curvature, which went from 0.63 preoperatively to 0.84 postoperatively and the maximum left iliac curvature, which went from 0.58 preoperatively to 0.81 postoperatively. The absolute differences between both observers was less than 16.5 m^{-1}. Only the pre-EVAR maximum left iliac

curvature had a high variability, namely 28.5 m^{-1} with an IQR of -5 m^{-1} to 66 m^{-1}. The other curvature differences were <16.5 m^{-1}.

Table 2-3 Interobserver variability curvatures pre-EVAR and post-EVAR

		Observer 1	Observer 2	Difference O1-O2	ICC	P-value
		Pre-EVAR				
Suprarenal curvature (m^{-1})	**Av**	13.0 [6 24]	7.5 [5 20]	2.0 [-1 7]	0.84 [0.58 0.94]	<.001
	Max	26.0 [12 47]	18.5 [9 44]	-0.5 [-9 15]	**0.68 [0.12 0.88]**	.02
Infrarenal curvature (m^{-1})	**Av**	20.0 [15 35]	17.0 [11 23]	3.5 [-1 14]	0.77 [0.37 0.91]	<.001
	Max	36.5 [25 57]	29.0 [23 38]	4.0 [-7 20]	0.80 [0.46 0.92]	<.001
Aneurysm curvature (m^{-1})	**Av**	23.5 [20 27]	18.0 [16 22]	5.0 [3 10]	**0.55 [-0.18 0.84]**	.01
	Max	53.0 [37 69]	44.5 [30 50]	11.5 [-1 21]	**0.63 [0.59 0.86]**	.01
Right iliac curvature (m^{-1})	**Av**	29.0 [24 33]	37.5 [28 46]	5.0 [0 9]	**0.75 [0.20 0.91]**	<.001
	Max	85.0 [58 111]	79.0 [54 96]	7.0 [1 14]	0.76 [0.37 0.91]	<.001
Left iliac curvature (m^{-1})	**Av**	37.5 [28 46]	30.0 [22 39]	5.0 [3 11]	0.85 [0.07 0.96]	<.001
	Max	100.0 [77 124]	68.5 [50 122]	28.5 [-5 66]	**0.58 [-0.03 0.84]**	.02
		Post-EVAR				
Suprarenal curvature (m^{-1})	**Av**	11.5 [9 20]	9.0 [7 12]	2.0 [1 7]	**0.66 [0.06 0.88]**	<.001
	Max	29.0 [18 43]	21.5 [16 31]	2.0 [-2 9]	**0.74 [0.32 0.90]**	<.001
Infrarenal curvature (m^{-1})	**Av**	22.5 [18 30]	18.0 [7 28]	3.5 [0 11]	0.81 [0.51 0.93]	<.001
	Max	42.5 [24 47]	28.0 [15 40]	7.0 [-4 18]	0.78 [0.41 0.92]	<.001
Aneurysm curvature (m^{-1})	**Av**	15.0 [13 22]	13.5 [10 16]	3.5 [1 5]	**0.55 [-0.11 0.83]**	.02
	Max	46.5 [30 62]	47.5 [33 59]	7.5 [-14 14]	0.84 [0.58 0.94]	<.001
Right iliac curvature (m^{-1})	**Av**	32.5 [29 39]	30.0 [19 39]	5.5 [-1 11]	0.79 [0.45 0.92]	<.001
	Max	66.5 [53 76]	59.5 [44 69]	8.0 [-8 27]	**0.64 [0.11 0.86]**	.01
Left iliac curvature (m^{-1})	**Av**	33.0 [19 45]	30.0 [20 38]	1.0 [-1 8]	0.89 [0.72 0.96]	<.001
	Max	75.0 [26 97]	50.5 [38 79]	16.5 [-9 24]	0.81 [0.51 0.93]	<.001

Values are presented as median [Q1 Q3]. ICC is presented with 95% confidence interval boundaries. ICC's below the threshold value of 0.75 are bold. Av, Average; ICC, intraclass correlation coefficient; Max, maximum; O1, observer 1; O2, observer 2.

The ICCs below the threshold value were further investigated by reviewing the curvature visualization of the individual outliers. Three findings are explained and shown with examples. Figure 2-6 shows the aorta of a patient with a severely angulated infrarenal neck, with protrusions. Observer 1 followed the curves of the neck while observer 2 drew a rather straight line resulting in higher maximum curvatures in the infrarenal neck for observer 1 when compared to observer 2 (123 m^{-1} and 74 m^{-1}, respectively). Furthermore, the renal arteries are at about the same height in the curve of the aorta. Observer 1 chose the left renal artery as baseline while observer 2 chose the right renal artery, resulting in a different level of the baseline. Therefore, the curve falls in the infrarenal segment for observer 1, but in the suprarenal and infrarenal segment for observer 2. This results in a maximum suprarenal curvature of 28 m^{-1} for observer 1 and 82 m^{-1} for observer 2.

Figure 2-7 shows an example of a patient in which the average curvature in the aneurysm segment differed between observer 1 and observer 2. Observer 1 chose to follow the curves of the asymmetry while observer 2 drew a more straight line. Observer 1 measured an average curvature of 35 m^{-1} in the aneurysm segment while observer 2 measured an average curvature of 18 m^{-1}. The curve of the proximal part in the aneurysm segment causes a rather small difference in the maximum curvatures, namely 74 m^{-1} for observer 1 and 67 m^{-1} for observer 2.

Figure 2-8 shows an example of a patient in which the maximal curvature in the left common iliac artery segment showed a big difference between observer 1 and observer 2 (64 vs 19 m^{-1}, respectively). From the figure it cannot be explained why observer 1 measured a larger curvature in the common iliac artery, but examining the 3D measurement in 3mensio revealed that the curvature difference arose in the bifurcation of the internal iliac artery. Figure 2-9 shows a schematic representation of the situation. Observer 1 induces an abrupt change in curvature while observer 2 induces a smooth transition from common iliac artery to the external iliac artery.

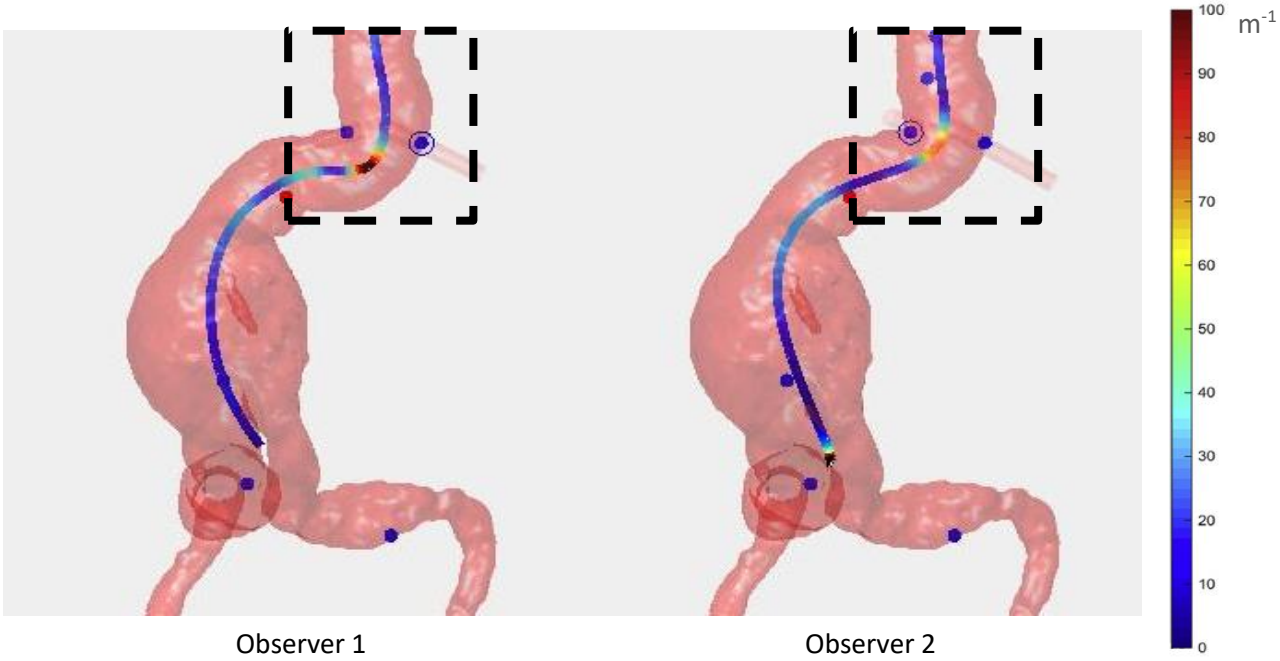

Figure 2-6 Example of difference between observer 1 (left) and observer 2 (right) in maximum curvature calculations on a pre-EVAR aortic center luminal line (CLL) *The colors of the CLL correspond to the curvature in m^{-1} indicated in the color bar. The box emphasizes a difference in curvature between the two observers in the infrarenal and suprarenal segment. The blue dots represent the reference markers. The circled dot represents the lowest renal artery marker. The red dot represents the end of the infrarenal neck.*

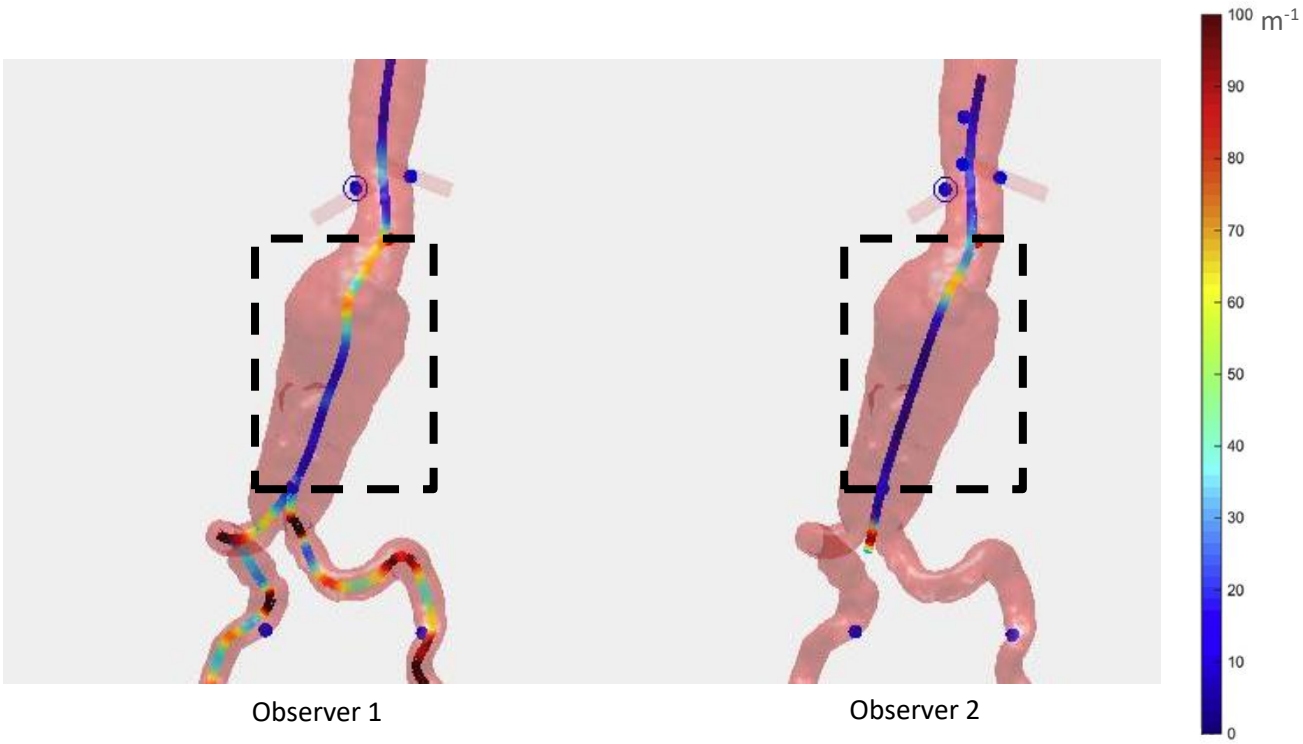

Figure 2-7 Example of difference between observer 1 (left) and observer 2 (right) in average curvature calculations on a pre-EVAR aortic center luminal line (CLL) *The colors of the CLL correspond to the curvature in m-1 indicated in the color bar. The box emphasizes a difference in curvature between the two observers in the aneurysm segment. The blue dots represent the reference markers. The circled dot represents the lowest renal artery marker. The red dot represents the end of the infrarenal neck.*

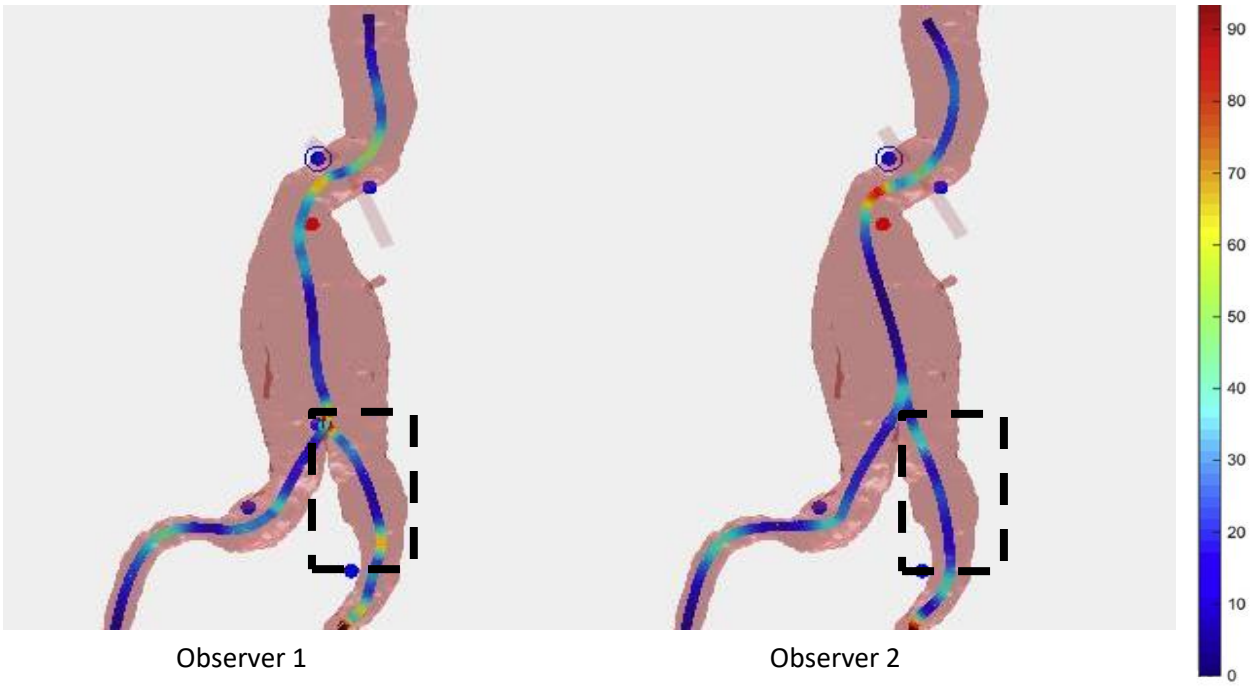

Figure 2-8 Example of difference between observer 1 (left) and observer 2 (right) in maximum curvature calculations on a pre-EVAR iliac center luminal line (CLL) *The colors of the CLL correspond to the curvature in m^{-1} indicated in the color bar. The box emphasizes a difference in curvature between the two observers in the left iliac segment. The blue dots represent the reference markers. The circled dot represents the lowest renal artery marker. The red dot represents the end of the infrarenal neck.*

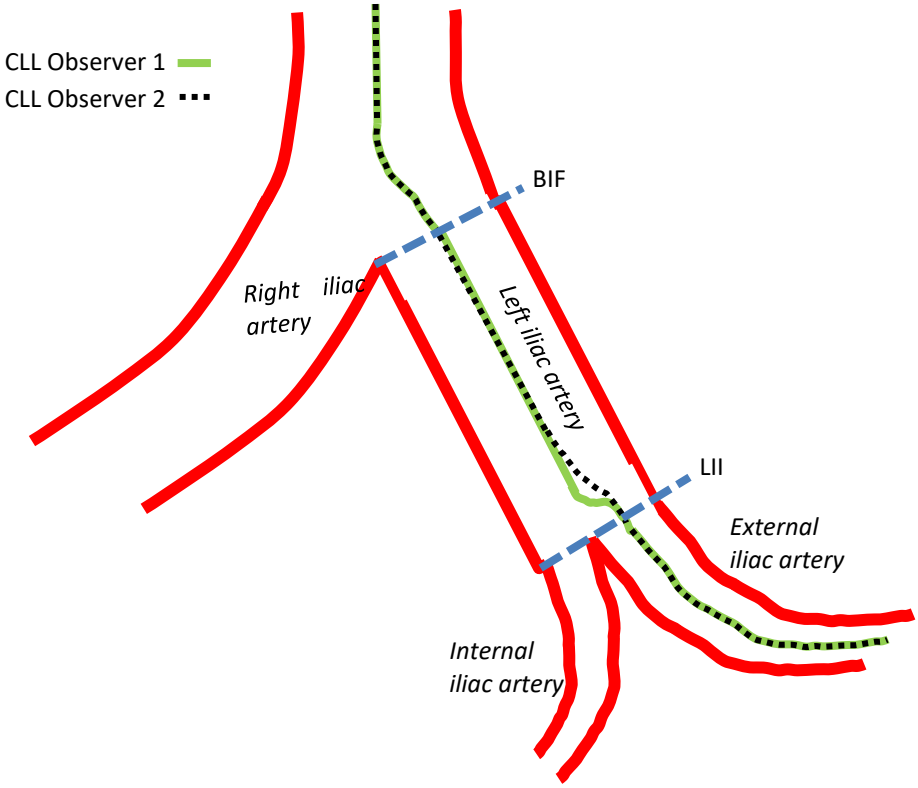

Figure 2-9 Schematic drawing of an example of different interpretation of the center luminal line (CLL) between observer 1 and observer 2 at the iliac bifurcation. *Curvature is calculated over the left iliac segment defined as the segment between the aortic bifurcation (BIF) and the left internal iliac artery (LII).*

2.3.3 Intraobserver variability

Diameters, neck length and angulations

Excellent agreement was observed for all dimensional measurements (ICC 0.89 - 0.99). The median differences between both measurements were <1.9 mm for the diameters, 0.4 mm for the neck length and < 1° for the angles.

Table 2-4 Intraobserver variability geometric measurements

Structure	Measurement 1	Measurement 2	Difference M1-M2	ICC	P-value
Baseline diameter (mm)	23.0 [21.3 24.2]	23.9 [22.0 25.4]	-0.9 [-1.8 -0.7]	0.91 [0.40 0.98]	<.001
End neck diameter (mm)	25.2 [23.5 27.0]	26.2 24.3 28.2	-1.0 [-2.2 -0.5]	0.89 [0.34 0.97]	<.001
Maximum aneurysm diameter (mm)	58.9 [55.8 65.0]	58.8 [56.4 66.3]	-0.6 [-1.5 -0.3]	0.99 [0.96 0.10]	<.001
Neck length (mm)	17.1 [10.5 32.6]	16.6 [10.0 34.6]	-0.4 [-3.6 1.5]	0.97 [0.93 0.99]	<.001
Alpha angle (°)	33.0 [24.0 54.0]	38.5 [26.0 58.0]	-1.0 [-7.0 2.5]	0.97 [0.93 0.99]	<.001
Beta angle (°)	60.5 [44.5 69.0]	[55.0 [47.5 70.5]	0.5 [-5.0 6.5]	0.93 [0.83 0.97]	<.001

Measurements and measurement differences are presented as median [Q1 Q3]. ICC is presented with 95% confidence interval. ICC, intraclass correlation coefficient; M1, Measurement 1; M2, Measurement 2.

Curvatures

Figure 2-10 shows that the preoperative ICCs of the average suprarenal curvature and the average and maximum aneurysm curvature were below the threshold value of 0.75. The same segments were below threshold value postoperatively with addition of the maximum suprarenal curvature. The median differences between measurement 1 and measurement 2 were all below 14 m^{-1}.

Table 2-5 Intraobserver variability curvatures pre-EVAR and post-EVAR

		Measurement 1	Measurement 2	Difference O1-O2	ICC	P-value
		Pre-EVAR				
Suprarenal curvature (m^{-1})	**Av**	7.5 [5 20]	18.0 [15 23]	-8.0 [-13 -5]	**0.70 [-0.20 0.92]**	<.001
	Max	18.5 [9 44]	27.5 [23 50]	-11.0 [-16 -3]	0.92 [0.65 0.97]	.02
Infrarenal curvature (m^{-1})	**Av**	17.0 [11 23]	26.5 [16 32]	-7.5 [-11 -5]	0.76 [0.25 0.92]	<.001
	Max	29.0 [23 38]	41.5 [24 54]	-8.0 [-18 7]	0.82 [0.51 0.93]	<.001
Aneurysm curvature (m^{-1})	**Av**	18.0 [16 27]	24.0 [19 27]	-6.5 [-8 -2]	**0.69 [-0.18 0.91]**	.01
	Max	44.5 [30 50]	45.0 [32 66]	-5.5 [-15 0]	**0.67 [0.17 0.87]**	.01
Right iliac curvature (m^{-1})	**Av**	29.0 [24 33]	39.5 [27 44]	-7.0 [-12 -2]	0.76 [-0.09 0.93]	<.001
	Max	79.0 [54 96]	77.0 [58 91]	-4.5 [-15 10]	0.87 [0.65 0.95]	<.001
Left iliac curvature (m^{-1})	**Av**	30.0 [22 39]	39.0 [31 48]	-8.5 [-16 -3]	0.81 [-0.08 0.95]	<.001
	Max	68.5 [50 122]	87.0 [54 114]	-14.0 [-21 -2]	0.92 [0.76 0.97]	.02
		Post-EVAR				
Suprarenal curvature (m^{-1})	**Av**	9.0 [7 12]	16.0 [14 20]	-7.0 [-12 -5]	**0.41 [-0.20 0.78]**	<.001
	Max	21.5 [16 31]	26.5 [23 43]	-7.5 [-12 -3]	**0.69 [0.19 0.88]**	<.001
Infrarenal curvature (m^{-1})	**Av**	18.0 [7 28]	23.5 [17 31]	-7.5 [-12 -2]	0.75 [0.33 0.91]	<.001
	Max	28.0 [15 40]	38.0 [24 56]	-10.5 [-16 3]	0.75 [0.35 0.90]	<.001
Aneurysm curvature (m^{-1})	**Av**	13.5 [10 16]	20.5 [18 22]	-7.0 [-8 -5]	**0.37 [-0.13 0.76]**	.02
	Max	47.5 [33 59]	44.5 [30 56]	5.5 [-1 19]	**0.55 [-0.24 0.83]**	<.001
Right iliac curvature (m^{-1})	**Av**	30.0 [19 39]	36.0 [29 41]	-7.0 [-8 -1]	0.88 [0.37 0.97]	<.001
	Max	59.5 [44 69]	58.0 [47 70]	-2.0 [-15 13]	0.84 [0.59 0.94]	.01
Left iliac curvature (m^{-1})	**Av**	30.0 [20 38]	34.5 [31 38]	-3.5 [-9 1]	0.88 [0.53 0.96]	<.001
	Max	50.5 [38 79]	68.5 [34 80]	-10.0 [-16 4]	0.83 [0.54 0.93]	<.001

Values are presented as median [Q1 Q3]. ICC is presented with 95% confidence interval boundaries. ICC's below the threshold value of 0.75 are bold. Av, Average; ICC, intraclass correlation coefficient; Max, maximum; M1, Measurement 1; M2, Measurement 2.

The ICCs below threshold were further investigated by analyzing the curvature visualization of the individual outliers. Figure 2-10 shows an example of a post-EVAR scan in which the average and maximum aneurysm curvature was higher for the second measurement. In the first measurement, the observer did not follow the sharp bend of the aorta but chose for a smooth transition. In the second measurement the center of the lumen was followed more accurately resulting in a sharper bend and thus a higher maximum curvature namely, 36 m^{-1} for measurement 1 and 85 m^{-1}.

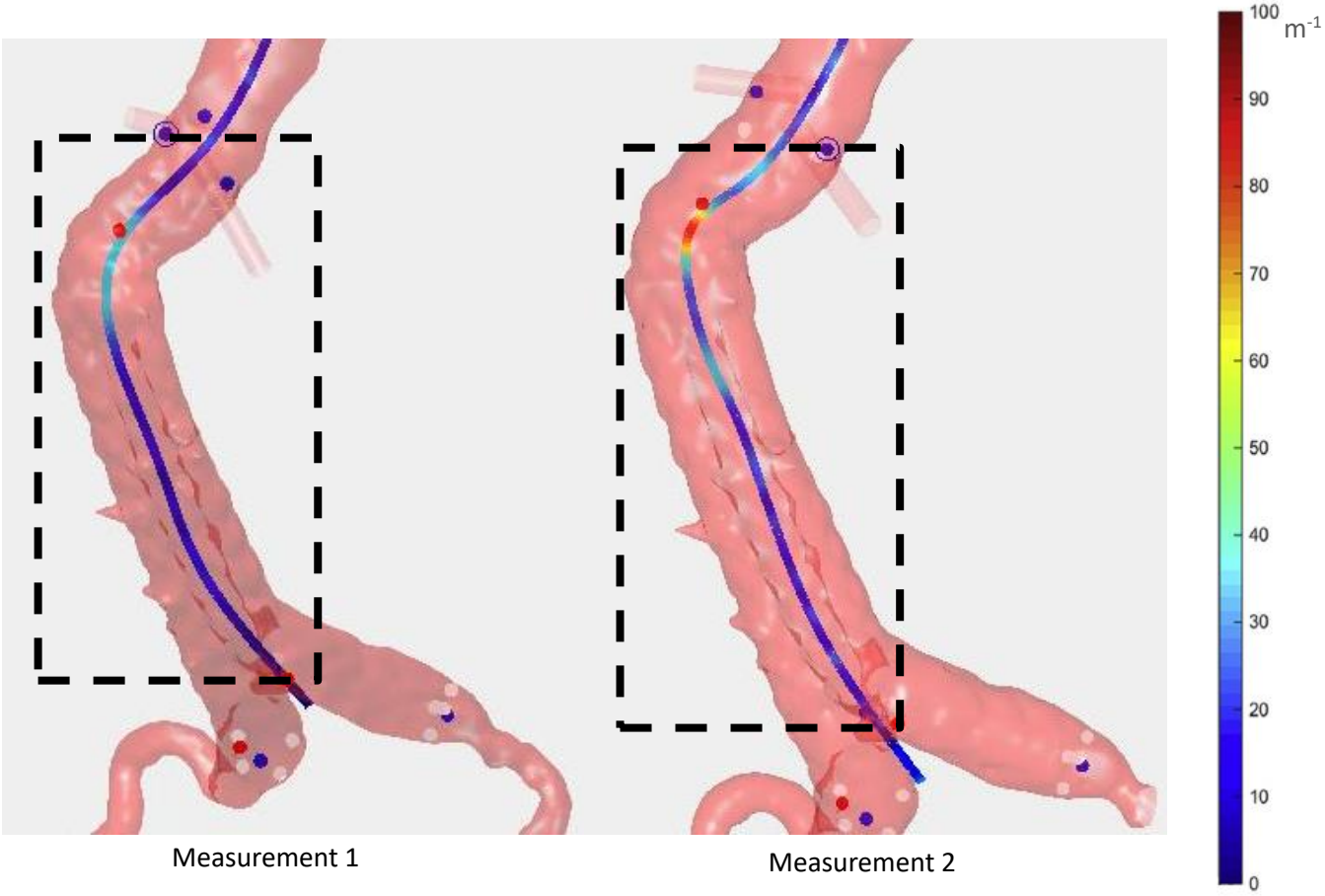

Figure 2-10 Example of difference between measurement 1 (left) and measurement 2 (right) in maximum calculations on a post-EVAR aortic center luminal line (CLL) *The colors of the CLL correspond to the curvature in m^{-1} indicated in the color bar***.** *The box emphasizes a difference in curvature between the two observers in the aneurysm segment. The blue dots represent the reference markers. The circled dot represents the lowest renal artery marker. The red dot represents the end of the infrarenal neck*

2.4 Discussion

This study revealed that the intra- and interobserver variability for curvature was moderate. Hence, curvature cannot be measured accurately by non-experienced observers. However, the intra- and interobserver variability of dimensional measurements was excellent. Diameters could be measured with a median variability of ≤1 mm for intra and inter observer variability. Median neck length difference was found 0.0 for interobserver variability and 0.4 mm for intra observer variability. Alpha and beta angulation differed on average 2.0° and 4.5° for interobserver variability and 1.0° and 0.5° for intra observer variability, respectively.

To the best of our knowledge, this is the first study reporting the observer variability in curvature calculations. A study by Schuurmann et al.(41) compared aortic neck curvature by automatic curvature calculation, semi-automatic curvature calculation by digital calipers, and aortic neck angulation. These methods were based on a CLL in 3Mensio drawn by two experienced observers. Although the variability between the methods was determined, the variability between both observers was not assessed. It is therefore not known if these observers agree on the creation of the CLL. Curvature is calculated at every point along the CLL. Therefore, the centerline must be drawn with great accuracy. Although there is no literature available yet on the intra- and interobserver variability of the aortic curvature, studies have reported intra- and interobserver variabilities of other parameters that were based on a CLL as well (60,61) Although the observer agreement was high in these studies, these results do not give a definite answer about the accuracy of the CLL because the measurements only represent a small part of the CLL. Curvature is calculated along the CLL, so accuracy of the whole CLL trajectory should be assessed. The results in this study confirm this statement as the excellent agreement in dimensional measurements was accompanied with moderate agreement in curvature. The absolute differences of the lengths and diameters were small and comparable with previous reported literature (55,62). Moreover, Ghatwary et al.(62) had similar measurements performed by a first-year medical student, which were comparable to the measurements of experts, implying that experience might not be a key factor in measuring lengths and diameters which is consistent with our results. The intra- and interobserver variability for the alpha and beta angulation in previous literature was 0.2° and 1.5°, respectively for alpha and 0.6° and 6.9°, respectively for beta (63). This study showed similar variabilities, namely an intra- and interobserver variability for alpha of 1.0° and 2.0°, respectively and for beta 0.5° and 4.5°, respectively.

In this study, some ICCs of curvature calculations were found below the preset threshold value of 0.75. An explanation may be found in outliers that were present. These could be caused in part by the predefined protocol that was subject to interpretation of the observer. Different interpretations led to observer variabilities, as depicted in Figure 2-6, Figure 2-7, Figure 2-8 and Figure 2-10. Furthermore, even though the protocol was used an validated in previous studies, measurements in those studies were performed by experienced observers (41,51,55). Therefore, the learning curve of both observers may have played a role in the outliers in this study. The five test-scans that were used as practice material may not have been sufficient for challenging anatomies. A training with meticulous measurement protocol, as used by observer 2, should be set-up on how to draw an accurate CLL. This protocol is a more detailed version of the protocol used by observer 1 to limit the observers interpretation. Furthermore, outliers in the intraobserver variability could be caused by the feedback obtained during the interobserver variability analysis, which preceded the intraobserver measurements. This explanation is substantiated by the absolute differences between observer 1 and observer 2 (Table 2-3), compared to the difference between both measurements of observer 2 (Table 2-5). The negative differences between observer 1 and observer 2 imply that observer 1 measured higher curvature than observer 2. The same phenomena is shown in the differences between the first and second measurement of observer 2 suggesting that observer 2 changed strategy to following the aortic wall more often, resulting in higher curvatures. Figure 2-10 shows

an example of such case. Additionally, some outliers were caused by a difference in marker placement. The protocol strictly described where all markers should be placed, but did not determine where the baseline should be placed when renal arteries are at the same height. This does not necessarily lead to a difference in marker location, as shown in Figure 2-10. However, when the renal arteries are located in the curve of the neck, as depicted in Figure 2-6, this can lead to a significant different determination of the surrounding segments. Depending on in which segment the maximum curvature of the curve will be, this can result in a major curvature change. Finally, outliers may be caused by patients with a severe asymmetrical angulated aortic anatomy. Optimal position of the CLL is hampered in an aorta with protrusions. When the protrusions are angulated creation of the CLL is even harder. Figure 2-6 shows an example of an aneurysm with a severely angulated and asymmetrical neck and the resulting curvature differences between observers.

A possible limitation of this study was the missing data in the scan protocol. The voxel size was not reported which could have placed the outcomes in better perspective. Moreover, the retrospective design may be considered a limitation as well. Observer 1 performed 106 measurements while observer 2 measured 20 patients, leading to imbalances of the observers experience. When performing an interobserver study, both observers should start with the same experience and the same goal of the measurements to reduce observer differences based on experience. Despite the experience imbalances, dimensional measurements can still be determined with excellent agreement. Furthermore, considerable limitation may be the intraobserver variability of observer 1 that was not assessed, so the reproducibility of this observers measurements is unknown. Another limitation in this study was the small sample size. More patients were not included due to a limited time frame in this thesis. It is possible that the ICCs that are just above or just below the threshold value will cross the threshold value when more patients are included. Furthermore, the agreement between both observers was hampered by outliers which are explained above. After elimination of these outliers the agreement between observers is expected to be sufficient, though this would make the sample size even smaller.

Conclusion

We found moderate agreement between the curvature measurements of two unexperienced observers, though these findings should be interpreted with caution considering the study limitations. Nevertheless, high observer agreement was found in diameters, neck length and angulation measurements. It is recommended to implement a training given by experts on how to draw a correct CLL, especially in asymmetrical aortas. Furthermore, a measurement protocol should be established with specific detail to how to draw a CLL in more complex anatomies. Appendix A can be used as basis. After such training a new intra- and interobserver study should be performed to obtain the variability between observers for curvature.

3 Aortic remodeling after EVAR: Anaconda vs Endurant

3.1 Introduction

Detailed knowledge about aortic remodeling after EVAR may help understand endograft failure and consequently improve the future generation endograft designs. Aortic remodeling can be expressed by a combination geometric properties such as changes in aortic diameters or curvatures. However, the intra- and interobserver variability in this thesis showed low observer agreement. Therefore, the aortic remodeling could not be determined by curvature. Koenrades et al.(64) examined aortic remodeling in diameters at different levels of the perirenal aortic neck. During two years of follow-up, they found no remodeling in the suprarenal aorta, a diameter increase in the infrarenal neck at the level of the sealing rings and a diameter decrease in the infrarenal neck at the level below the sealing rings. A decrease in diameter in the infrarenal neck below the sealing rings may positively affect the sealing and fixation of the endograft (56). This study was limited by its small sample size. The current study included a bigger cohort of Anaconda patients to assess aortic remodeling in aortic neck diameters. Moreover, this study compared the Anaconda endograft with an endograft using a different proximal sealing mechanism, namely the Endurant endograft. The Anaconda endografts contain a flexible main body with proximal two saddle-shaped nitinol rings, with four pairs of sealing hooks while the endurant uses a main body with nitinol M-shape stent design and suprarenal anchor pins to provide proximal sealing (38,39). In section 1.2.4 more details are described on the differences between the two endografts. The aim of this study was to examine difference in remodeling after EVAR between the Anaconda and Endurant endograft by analyzing the changes in diameters of the aortic neck.

3.2 Methods

3.2.1 Study Design

In this retrospective study, aortic remodeling was assessed in CTA scans patients with an asymptomatic infrarenal AAA who underwent elective EVAR. 79 patients were treated with an Anaconda endograft and 124 patients were treated with an Endurant endograft. The Anaconda patients (mean age 74 ± 9 years; male gender 55 (85.9%)) were retrospectively enrolled between December 2014 and December 2018 in an observational multi center cohort study: Limb Occlusion Predictive Value of postoperative Angulation Changes on CT of Anaconda endografts (LOPVACTA). This study included patients who received an Anaconda endograft in the Diakonessenhuis hospital in Utrecht, the Netherlands. The current study included of each patient with an asymptomatic infrarenal AAA, the pre-EVAR and first post-EVAR CTA scan. Patients without contrast were excluded. Patients who received a stent prior to EVAR were excluded as well. Moreover, patients with missing CTA data or patients that could not be loaded into 3Mensio were excluded. At last, patients who received the pre-EVAR scan >1 year before EVAR or patients who received the post-EVAR scan >6 months after EVAR were excluded. From the Anaconda cohort, fourteen patients scanned without contrast were excluded, one patient who received an endograft prior to EVAR and was excluded and one patient did not have an infrarenal AAA and was therefore excluded. Details of the Endurant patient cohort were described previously (56). Initially, the 124 EVAR patients were included. From the Endurant cohort. Two patients were excluded because of missing data. Twelve scans could not loaded into 3Mensio and were therefore excluded. Moreover, one patient was excluded because the pre-EVAR scan was made 4 year for EVAR. 3 measurements were missing in the obtained data. Figure 3-1 illustrates the patient selection of the current study.

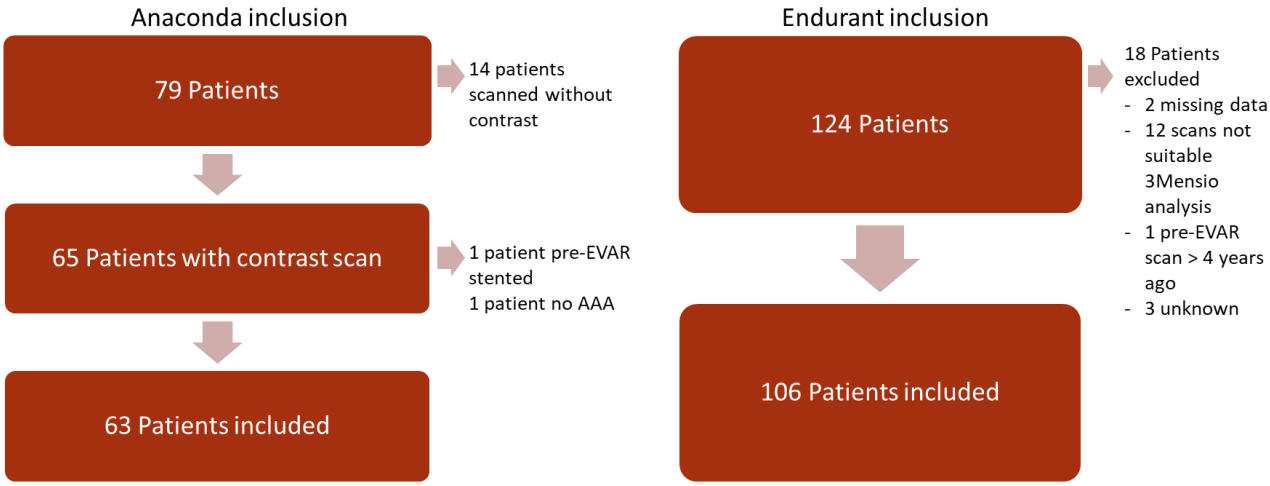

Figure 3-1 Flowchart indicating patient selection for Anaconda and Endurant
AAA, abdominal aortic aneurysm; CTA, Computed Tomography Angiography; EVAR, endovascular aneurysm repair

3.2.2 Image acquisition

All Anaconda CTA scans were performed on a Somatom Definition AS scanner (Siemens Healthineers, Erlangen, Germany). The scan parameters included: rotation time 0.5 seconds, tube potentials 120 kV, tube current 60 mAs, collimation 64x0.6 mm, pitch factor 1.4, reconstruction matrix size 512x512 pixels and slice thickness ranged between 1.0-3.0 mm, depending on scan protocol. All scans were performed during inspiration breath hold. Data were reconstructed with a I41f\2 convolution kernel

The scan protocol of the Endurant cohort has been described in section 2.2.2.

3.2.3 Measurement protocol

The measurement protocol has been described in section 2.2.3. In short the following preoperative parameters were measured: baseline diameter, end of neck diameter, aneurysm diameter, neck length, alpha angle and beta angle. Additionally, diameters were measured to define the aortic remodeling in the supra-, juxta- and infrarenal neck at predefined levels: (A) 30 mm above the baseline, (B) 15 mm above the baseline, baseline, (D) 5 mm below baseline and (E) 10 mm below baseline, as shown in Figure 3-2. Levels were located along the CLL.

3.2.4 Statistical Analysis

Shapiro-Wilk tests were used to assess normality of the continuous data. Normally distributed data was presented as mean ± standard deviation (SD); skewed data was presented as median with interquartile range (IQR). Mann-Whitney U tests were used to indicate significant differences between the pre- and post-operative scans and between the Anaconda and Endurant endografts. P-values <0.05 were considered significant. Statistical analyses were performed using IBM SPSS Statistics for Windows (version 25.0; IBM Corporation, Armonk, NY, USA).

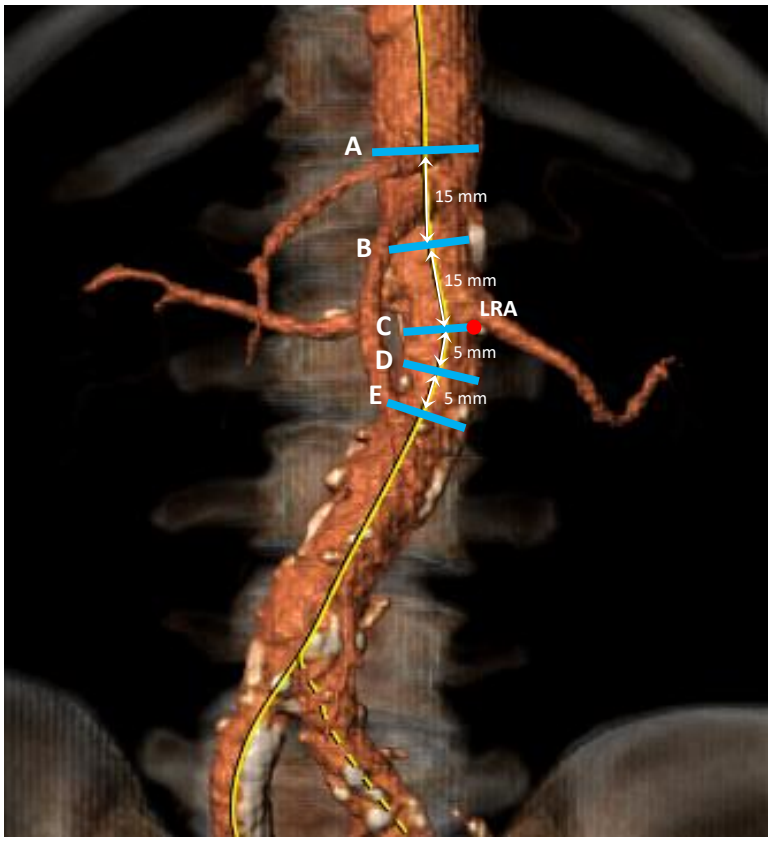

Figure 3-2 Schematic presentation of five aortic levels relative to the baseline
Diameters were measured orthogonal to the baseline at A; 30 mm above baseline, B; 15 mm above baseline, C; Baseline, D; 10 mm below baseline, E; 10 mm below baseline

3.3 Results

3.3.1 Baseline patient characteristics

The baseline characteristics and preoperative morphologic characteristics are shown in Table 3-1. Thrombus and calcification was significantly different between both cohorts. The Endurant cohort had more moderate aortic neck thrombus and mild calcification than the Anaconda cohort (*P*<.001). Hyperlipidemia tobacco use and cardiac disease were unknown of the Endurant cohort. Median main body oversizing of the Anaconda and the Endurant cohort were 17.0% [IQR 14.0 26.0], and 19.2% [IQR 12.9 26.6], respectively.

3.3.2 Neck diameters

Table 3-2 presents the postoperative change in diameters at different aortic levels for the Anaconda and Endurant patients. The preoperative diameters were not significantly different between both cohorts at all levels. The aortic diameters of the Anaconda cohort did not significantly change from pre- to postoperatively at all levels, while the diameters for the Endurant patients significantly increased at all levels except at 30 mm above the baseline.

Table 3-1 Baseline patient characteristics and preoperative morphologic characteristics

	Anaconda (n=63)	Endurant (n=106)	P-value
Baseline patient characteristics			
Age	73.3 ± 8.9	74.4 ± 7.2	.11
Male gender	55 (87.3)	93 (87.7)	.93
Hypertension	21 (33.3)	47 (69.8)	.13
Hyperlipidemia	41 (65.1)	-	-
Tobacco use	24 (39.3)	-	-
Diabetes mellitus	12 (19.0)	19 (21.7)	.90
Cardiac disease	27 (42.9)	-	-
Pulmonary disease	19 (30.2)	23 (21.7)	.25
Renal disease	10 (15.9)	61 (75.3)*	**<.001**
Preoperative morphologic characteristics			
Neck thrombus			
• Absent	61 (96.8)	50 (47.2)	**<.001**
• Mild	2 (3.2)	33 (31.1)	**<.001**
• Moderate	0 (0.0)	23 (21.7)	**<.001**
Neck calcification			
• Absent	62 (98.4)	69 (65.1)	**<.001**
• Mild	1(1.6)	31 (29.2)	**<.001**
• Moderate	0 (0.0)	6 (5.7)	0.053
Neck shape			
• Straight	34 (55.7)	64 (60.4)	.37
• Conical	20 (29.5)	36 (34.0)	.74
• Reversed conical	2 (3.3)	3 (2.8)	0.91
• Dumbbell	7 (11.5)	3 (2.8)	**0.03**
Baseline at accessory renal artery	3 (4.9)	10 (9.4)	.26
Maximal aneurysm diameter	60.9 [54.7 68.1]	59.0 [55.0 67.0]	.59
Neck length	23.1 [18.0 39.0]	23.5 [13.0 35.3]	.26
Alpha angle	26.0 [16 40.0]	30.5 [19.0 43.5]	.17
Beta angle	41.0 [28.0 60.0]	52.0 [38.5 66.3]	**.013**
Aneurysm right iliac artery	11 (18.0)	45 (42.5)	**.001**
Aneurysm left iliac artery	9 (14.3)	37 (34.9)	**.003**
Stenoses>50% right iliac artery	13 (21.3)	5 (4.7)	**.001**
Stenoses>50% left iliac artery	18 (29.5)	3 (2.8)	**<.001**

**Renal disease of 25 Endurant patients was unknown.*

Data shown as median [interquartile range] or number (%).

Table 3-2 Diameters changes in the aortic neck

	Aortic level	+30 mm	+15 mm	Baseline	-5 mm	-10 mm
Anaconda	Diameter pre-EVAR (mm)	26.4 ± 2.5	25.6 ± 2.3	24.8 ± 2.5	25.4 ± 2.6	25.1 ± 2.8
	Diameter post-EVAR (mm)	26.4 ± 2.7	25.7 ± 2.4	25.2 ± 2.8	25.1 [22.8 28.0]	25.0 ± 3.2
	Diameter Change post-pre (mm)	-0.1 [-0.6 0.5]	-0.1 [-0.7 0.5]	0.2 [-0.7 1.1]	0.6 ± 2.1	0.0 [-1.2 1.0]
	P-value	.86	.81	.38	.43	.70
Endurant	Diameter pre-EVAR (mm)	26.0 [24.8 28.2]	25.0 [23.7 27.2]	24.0 ± 2.3	24.1 ± 2.5	24.8 ± 2.8
	Diameter post-EVAR (mm)	26.4 [25.2 28.6]	26.2 [24.5 28.0]	24.5 ± 2.5	25.7 ± 2.4	26.3 [24.9 27.9]
	Diameter Change post-pre (mm)	0.2 ± 0.5	0.8 [0.1 1.5]	1.3 [0.7 2.3]	1.6 ± 1.1	1.5 [1 2.6]
	P-value	.47	**.010**	**<.001**	**<.001**	**<.001**
Anaconda vs Endurant	Diameter pre-EVAR P-value	.75	.46	0.064	0.067	0.284
	Diameter post-EVAR P-value	.40	.21	.35	.27	**.002**
	Diameter change post-pre P-value	**0.008**	**<.001**	**<.001**	**<.001**	**<.001**

Data are presented as mean ± standard deviation or as median [Q1, Q3] as appropriate for the distribution of the data. Aortic levels are defined with respect to the baseline. EVAR, endovascular aneurysm repair

3.4 Discussion

This study assessed aortic remodeling in two different endograft types, the Anaconda and the Endurant, by assessing the change in aortic neck diameters. The diameters of the Anaconda cohort remained stable, while the diameters in the Endurant cohort increased at all levels except at 30 mm above the baseline. No remodeling was expected at the level 30 mm above the baseline as this level is not (directly) affected by the endograft material. At 15 mm above the baseline, the aorta is not affected by the Anaconda endograft, as the saddle shaped sealing rings are deployed below the lowest renal artery, but suprarenal anchor pins of the Endurant induced a significant median diameter change of 0.8 at this level.

Progressive infrarenal aortic neck enlargement after insertion of an Endurant endograft has been reported previously (65,66). Savlovski et al. compared the changes in aortic neck diameters between the Endurant endograft and the Nellix endograft. Diameters were measured just below the superior mesenteric artery, and at three infrarenal levels; level 1, just below the lowermost renal artery; level 2, at the proximal end of the endograft fabric and level 3, 5 mm below the proximal end of the endograft fabric. The three infrarenal levels are similar to the baseline level, level at 5 mm below the baseline and level at 10 mm below the baseline that were used in the current study. Savlovski et al. found a statistical significant increase in the diameters of level 1 (1.80 mm) and level 2 (2.04 mm) on the first postoperative scan. Level 3 was not statistically different. The found increases are higher than the 1.3 and 1.6 mm in this study. A possible explanation could lie with the preoperative diameters that were higher by Savlovski et al. than the preoperative diameters found in this study at all levels. Other baseline characteristics are not shown and therefore the differences cannot be explained.

Previous literature showed that the Anaconda endografts induce a diameter increase in the infrarenal neck at the level of the sealing rings (64,67). Koenrades et al.(64) evaluated if the radial forces of the Anaconda sealing induced dilation in the aortic neck. During two years of follow-up, they found no remodeling in the suprarenal aorta, a diameter increase in the infrarenal neck at the level of the sealing rings and a diameter decrease in the infrarenal neck at the level below the sealing rings. This is contrary to our finding that the Anaconda diameters do not significantly change postoperatively. A possible explanation could be that the remodeling of the Anaconda rings is a process that occurs over a longer period. This study included only the first postoperative scan. The period between the pre- and post-EVAR CT scans was less than 6 months. More follow-up scans should be included to find out of the Anaconda rings increase over time. However, the diameter increase by the study of Koenrades et al.(64) was already detected after one month. Also, the infrarenal decrease reported by Koenrades et al.(64) was not observed in this study. This can be explained by the fact that only 2 diameters below the baseline were included in this study, that were near the sealing zone. To observe the decrease in diameter, more levels should be included in the renal neck caudal the sealing zone.

Oversizing was slightly higher in the Endurant cohort than the Anaconda cohort. Statistical differences could not be determined because the Endurant data was not available. The median value lies within the oversizing advised 10-20% oversizing in the instructions for use of both cohorts (38,39).

Limitations

The Endurant cohort and Anaconda cohort were not preoperatively matched, which is possible limitation. Preoperative anatomical characteristics might differ between these groups as they have a different range for patient inclusion. The preoperative morphologic characteristics showed that the Endurant cohort included patients with significantly larger beta angles than the Anaconda cohort. However, the preoperative diameters of both cohorts were not significantly different.

The Endurant measurements were performed previously by a second observer for a different study purpose. Due to time and technical limitations, measurements could not be added to these previously measured structures.

Moreover, only aortic diameters and curvatures were measured pre- and post-operatively by the Endurant observer. A previous study showed that the observer agreement on aortic curvature was low. Therefore, only the aortic diameters could be used to determine the postoperative aortic remodeling.

Another limitation could be the limited availability of data of the Endurant cohort. The patient group of 90 patients used by de Rooy (56) to assess adaptive neck enlargement could not be reconstructed due to missing data. De Rooy (56) excluded patients based on long distances between the renal arteries and the endograft fabric. This should have been included in this study as well. If the endograft is deployed lower than 10 mm below the lowest renal artery, it does not affect the set levels of aortic diameter measurements. The distance between the lowest renal artery and the endograft fabric was not retrievable from the data. Therefore this exclusion was not implemented for both cohorts. Nevertheless, although 106 patients were measured in this study instead of the 90 patients used by De Rooy, the diameter outcomes were similar. (At the aortic levels +30, +15 baseline, -5 and -10 he found a postoperative diameter change of 0.2 (-0.2 – 0.6), 0.8 (0.1 – 1.5), 1.3 (0.7 – 2.3), 1.7 (0.9 – 2.5) and 1.6 (1.0 – 2.7) respectively).

Conclusion

This study showed that no aortic remodeling in diameters was observed in the Anaconda cohort, on the first post-EVAR CTA scan. Increased aortic diameters were found in the Endurant cohort at the level of 15 mm above the baseline, at the baseline, 5 mm below the baseline and 10 mm below the baseline. These results suggest that the Anaconda sealing and fixation complies better to the aortic wall while the Endurant anchor pins induces advance neck enlarged. Future research should more include follow-up scans to assess the aortic remodeling over time.

4 The influence on cardiac-pulsatility-induced motion detection calculation electrocardiographically-gated computed tomography angiography scans reconstructed into 8 or 10 cardiac phases

4.1 Introduction

In the previous chapters, several static measurements were described to investigate the geometrical changes that occur in the aorta after the placement of an endograft. In addition to the statical properties, it is important to examine the dynamics of the aorta, as the aorta is under constant influence of the pulsatile blood flow. The pressure changes of the pulsatile blood flow may challenge the fixation and sealing of the endograft. In addition, endografts generally stiffen the aortoiliac axis, especially in the case of highly angulated vessels, putting stress and forces on the endograft frame (69). This may lead to failure of the endograft sealing, resulting in migration and type 1 endoleak. As described in section 1.2.2, type 1 endoleaks allow blood flow into the aneurysm sac causing aneurysm repressurization, increasing the risk of rupture and therefore requiring reintervention. Preoperative high aneurysm neck pulsatility has been associated with postoperative endograft migration already (70). Moreover, examining the change dynamic behavior in the aorta caused by endografts can help improve the future generation endograft designs and predict endograft failure in individual patients (45,46). It is therefore important to investigate how aortic motion patterns may change after endograft placement and to examine potential relations between these motion patterns and complications. The motion patterns can be analyzed using retrospective electrocardiogram (ECG)-gated computed tomography angiography (CTA) scans.

A study within the present research line, quantitatively characterizes and compares the motion and geometry of two types of iliac branched devices (IBDs). The patient cohort with the first device was scanned with an ECG-gated CT scan protocol reconstructing 8 cardiac phases, while the patient cohort with the other device was scanned with an ECG-gated CT scan protocol reconstructing 10 cardiac phases, resulting in 8 or 10 CT volumes, respectively. Because 10 volumes contain more data and thus more detail, it is conceivable that small movements are captured in 10 phases reconstructions which are missed in 8 phases reconstructions. In order to compare the motion patterns and dynamic geometrical properties of the IBDs, it must be determined to what extent the phase difference produces a difference in measured motion.

In this thesis, an in vitro experiment was performed to compare motion calculations between 10 and 8 phases reconstructions of ECG-gated scans. Moreover, an explorative patient study was performed to evaluate the effect in clinical setting.

4.2 Methods

4.2.1 *In vitro experiment*

Study Design

For this study an in vitro experiment was performed to obtain a series of ECG-gated CT scans with a moving endograft at different frequencies. An in-house developed linear actuator device was used to obtain a controlled motion in one direction, see Figure 4-1. The motion is induced by a custom made coil (BEI, linear voice coil actuator LA18-12-007Z), with a stroke of 3 mm back and forth, so a top-top distance of 6 mm could be created. The actuator was excited by an Agilent HP 33120A arbitrary waveform generator (Agilent Technologies) connected to an oscilloscope for visual feedback. A GORE® EXCLUDER® AAA Endoprosthesis (Gore Excluder W.L. Gore & associates, Flagstaff, AZ, USA) was attached to the lever of the linear actuator. To trigger the CT scan an ECG-phantom (ProSim 8 Vital Signs and ECG Patient Simulator, Fluke Biomedical) was used. The ECG-phantom and linear actuator were not synchronized, due to technical limitations. To obtain an accurate ground truth for the motion of the prothesis, a Hall sensor (A1318LUA-2-T Allegro Microsystems, Hall Effect Sensors, 3-Pin SIP) was attached to the lever of the linear actuator. The Hall sensor was controlled by an Arduino microcontroller (Arduino, 5V 16M Mini Leonardo Microcontroller) programmed with a specialized Arduino C-code. Calibration of the microcontroller prior and after the measurement resulted in a measurement error of less than 0.1 mm of the Hall sensor. The sensor used a sample frequency of 100 Hz. The data from the sensor was read and analyzed with a specialized script in Processing (Processing 3.5.4 for Windows). The obtained amplitudes were further processed in Matlab (MATLAB R2020b The MathWorks, Natick Massachusetts, USA).

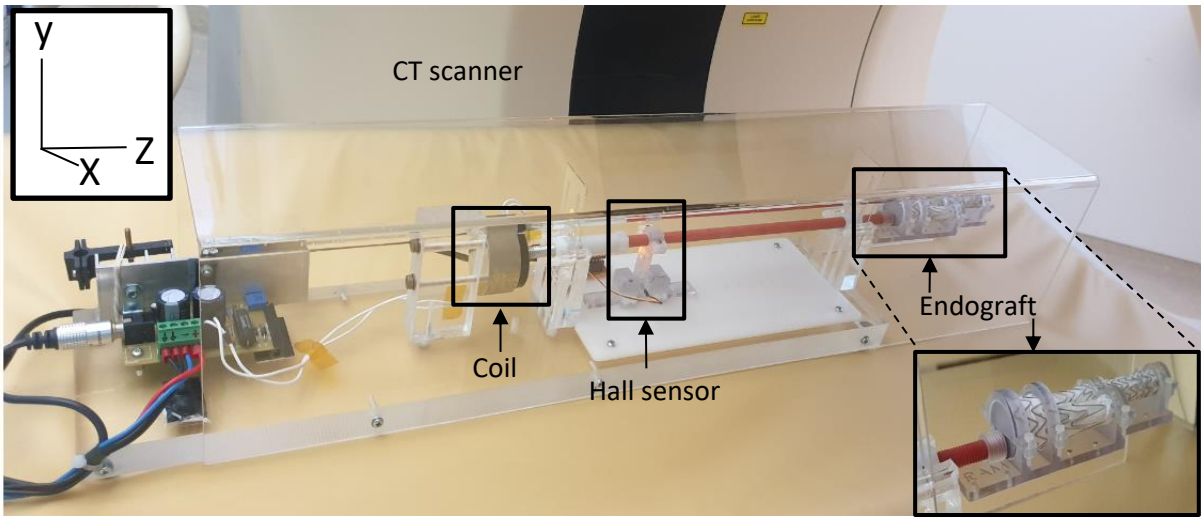

Figure 4-1. Experimental set up. *The coil of the linear actuator provided a linear movement in the z-direction. CT, computed tomography*

Generated motion patterns

The shape of a pressure profile in the aorta as reported by Hazer et al.(71) was programmed in the waveform generator, see Figure 4-2. This signal was used as input signal for the linear actuator to mimic the aortic motion. The amplitude was set at 50mV in the waveform generator, resulting in an in a stroke of 1.4 mm of the endograft. To study the influence of the heartrate, several CT scans were created using different frequencies, ranging from 50 to 100 beats per minute (BPM) with intervals of 10 BPM. A cardboard basin was placed under the linear actuator and it was placed diagonally to induce movement in the x- and y-direction as well as the z-direction. This 3D movement was studied at 60 and 70 BPM. Additionally, two measurements were performed using a sinusoidal wave at 50 BPM and 75 BPM.

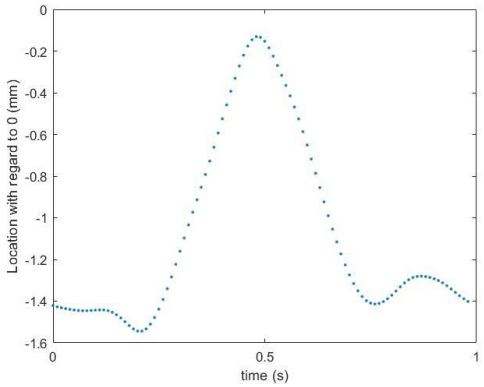

Figure 4-2 Illustration of the shape of the pressure profile in the aortic artery as reported by Hazer et al. (64)

Image acquisition

All ECG-gated CTA scans were performed on a 256-slice CT scanner (Brilliance iCT 256; Philips Healthcare, Best, The Netherlands) with a standardized protocol. Scan parameters were as follows: tube voltage, 120 kV; tube current time product, 86 mA·s; collimation, 80x0.625 mm; rotation time, 0.33 s; slice thickness, 1 mm; slice increment, 0.5 mm; reconstruction matrix, 512 x 512 pixels (voxel size xy × matrix size= 0.5 × 512); pitch factor, 0.16. The raw data was retrospectively reconstructed into 8 phases scans and 10 phases scans so that 8 or 10 equally sized phases of the cardiac cycle were obtained, from 0% to 87.5% or from 0% to 90% of the RR interval respectively. Technical limitations restricted reconstruction at 0.5%, so the 8 phases scan was reconstructed at 0%, 13%, 25%, 37%, 50%, 63%, 75% and 88% of the RR interval.

Image processing

Image processing was conducted using a specialized algorithm for image registration, which has been used previously to study endograft motion (33,48,49). The registration includes acquiring deformation fields for each reconstructed phase, describing the displacement of each voxel in all phases with respect to the average of all phases, allowing assessment of the motion patterns throughout the phases with a maximal error of 0.3 mm (49). The algorithm was created in Python programming language (version 3.7).

Markers

A set of 5 markers was manually selected at the same locations in both reconstructions. Of each marker the amplitudes of motion patterns in the z-direction and the total pathlength during the cardiac cycle was obtained. For the 3D measurements, the motions patterns of the x-, y- and z-direction were obtained. The pathlength was defined as the sum distances between subsequent locations of each markers during cardiac cycle. All markers were placed at the most cranial point of the M-shaped frame of the endograft, as shown in Figure 4-3. Marker 1 was selected at the top of the longest leg of the endograft, marker 2 was selected at the top of the shortest leg, marker 3 and marker 4 were selected on the ventral and dorsal side the main body and marker 5 was selected at the end of the endograft.

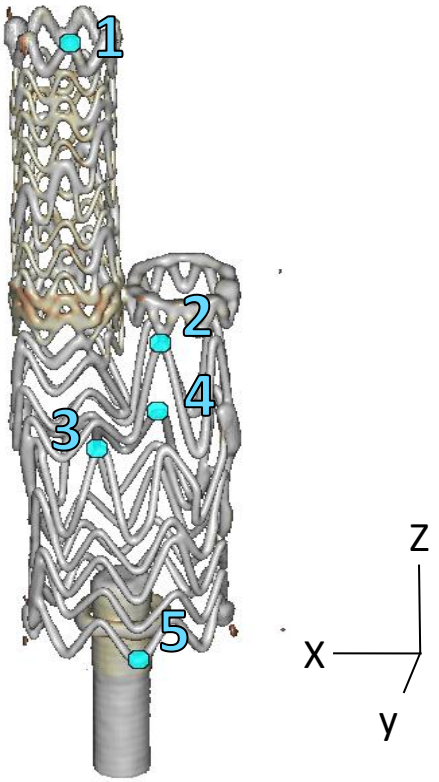

Figure 4-3. Marker placement on the endograft *All markers were placed at the most cranial point of the M-shaped frame of the endograft. Marker 1 was selected at the top of the longest leg of the endograft, marker 2 was selected at the top of the shortest leg, marker 3 and marker 4 were selected on the middle of the ventral (3) and dorsal(4) side the main body and marker 5 was selected at the end of the endograft*

Simulation

The linear actuator was not synchronized with the ECG-phantom. Since the linear actuator continuously performed the aortic pressure movement, the scanning started at a random amplitude of the induced pressure wave. Depending on the starting point, the top of the pressure wave could be skipped or included by both reconstructions. To assess this effect, a simulation was performed using the sensor output as basis signal. The samples of one cardiac cycle of the sensor signal were divided into 8 or 10 equal parts of consecutive samples. Of each part, the average value of the corresponding sensor output was determined, resulting in 8 or 10 averaged values representing the samples of the 8 or 10 phases reconstructions, respectively. These samples were used to construct the movement as detected by an 8 or 10 phases ECG-gated CT reconstruction. Figure 4-4 shows two examples of such construction for the 10 phases reconstruction.

For each possible starting point of the 8 and 10 phases reconstructions, the difference in pathlength was assessed. For each frequency the difference between the 8 and 10 phases scan was determined.

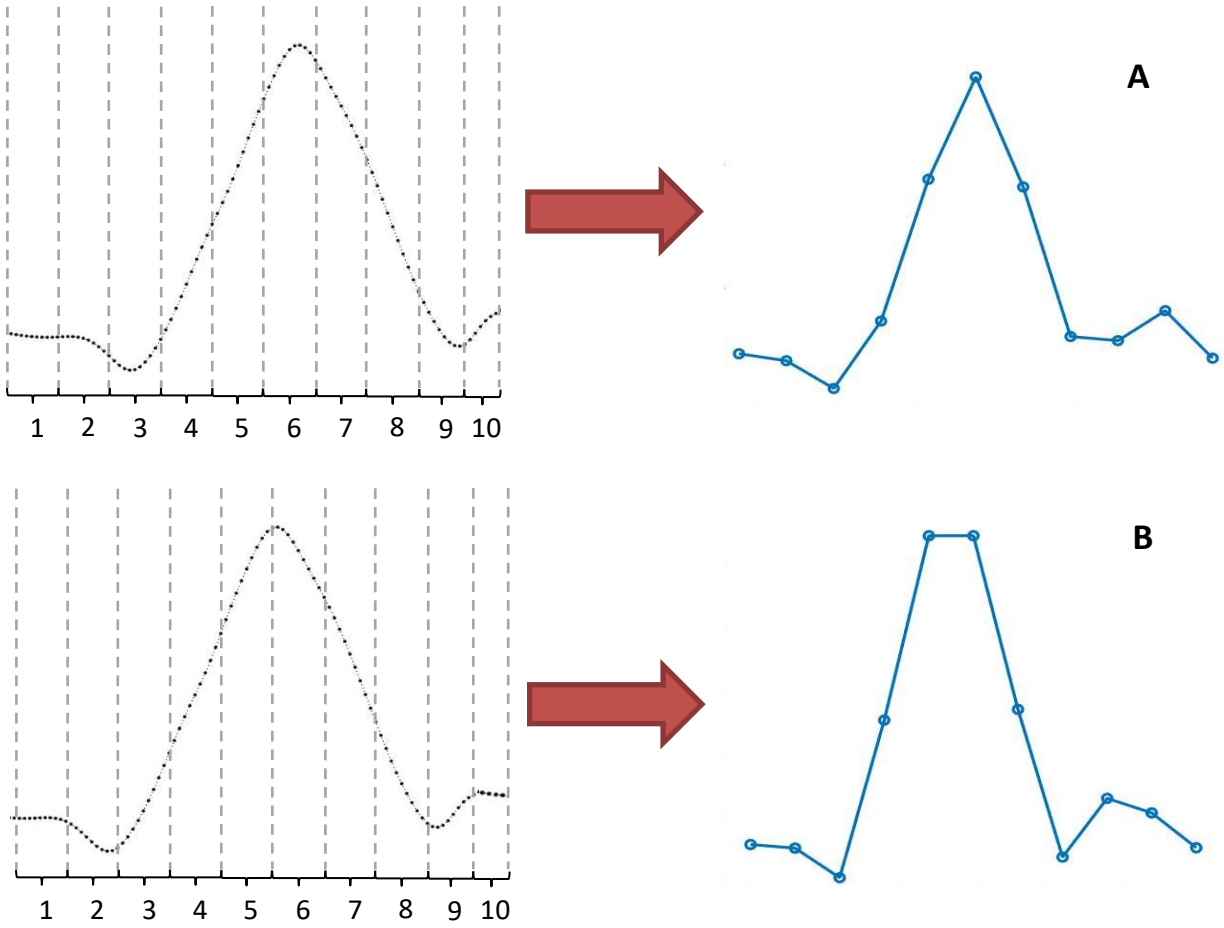

Figure 4-4 Two examples of the simulation of a 10 phases reconstruction *The samples of the sensor signal (dashed signal) were divided into 10 equal parts. In each part, the average value of the amplitude was calculated. The resulting 10 average values were used as samples to draw the 10 phases reconstruction (blue line). B shows an example that is 5 samples delayed on A.*

Statistical Analysis

Shapiro-Wilk tests were used to assess normal distribution of the continuous data. Normally distributed data was presented as mean ± standard deviation (SD); skewed data was presented as median with interquartile range (IQR). The differences between the 8 and 10 phases reconstructions were also presented as percentage of the 8 phases reconstruction. Paired sample T-tests were used to indicate significant differences between the pathlengths, minimum and maximum amplitudes of 8 phases and 10 phases reconstructions. P-values <0.05 were considered statistically significant. Statistical analyses were performed using IBM SPSS Statistics for Windows (version 25.0; IBM Corporation, Armonk, NY, USA).

4.2.2 Explorative patient study

Study Design

An ECG-gated CTA scan from a patient 12 months post-FEVAR, who received a 4-fenestrated aorto-bi iliac Anaconda endograft (Terumo-Aortic, Inchinnan, Scotland) was retrospectively included. This patient was enrolled in an observational single-center cohort study (Longitudinal Study to changes in shape and motion of the aorta and endoprosthesis after fenestrated endovascular aneurysm repair (LSPEAS F-EVAR), Trialregister.nl identifier: NTR6225)

Image acquisition

The ECG-gated CTA scans was performed on a Somatom Definition Flash CT scanner (Siemens Healthineers, Forchheim, Germany) with a standardized protocol. Administered contrast volume was 80 ml with a flow of 4ml/s. Scan parameters were as follows: rotation time, 0.3 seconds; collimation, 38.4 x0.6 mm; slice thickness, 1 mm; slice increment, 0.5 mm; tube voltage, 120 kV; tube current time product,(374 mA X-Ray Tube Current) mA·s; Data were reconstructed with a I36f\2 convolution kernel, a matrix size of 512 x 512 pixels, and a field of view of approximately 250 x 250 mm, resulting in isotropic voxels of 0.5 mm. The pitch factor was set automatically, based on the heart rate. Data reconstructions were obtained as described in section 4.2.1 *Image Acquisition.*

Image processing

The image processing steps are described in section 4.2.1 *Image Processing.*

Markers

To study the motion patterns, a set of markers was manually selected at the same locations in both reconstructions. The location of these markers was based on locations in which most motions were expected or based on practically manageable points on the stent frame, so that these markers are retrievable in other patients. Of each marker the motion patterns in the x-, y- and z-direction and the total pathlength during the cardiac cycle was obtained. The markers were placed at the following structures (See Figure 4-5):

1. The ventral side of the proximal ring of the Anaconda FEVAR cuff
2. The dorsal side of the proximal ring of the Anaconda FEVAR cuff
3. The proximal origin of coeliac trunk branch
4. The proximal origin of the superior mesenteric artery branch
5. The ventral side of the proximal ring of the Anaconda main body
6. The dorsal side of the proximal ring of the Anaconda main body
7. Ventral curve right iliac component
8. Ventral curve left iliac component

Statistical Analysis

Statistical analysis was performed as described in 4.2.1 *Statistical Analysis.*

4.3 Results

4.3.1 In vitro experiment

Motion patterns

Table 4-1 and Table 4-2 show the maximal motion amplitudes for each marker per heartrate. The maximum amplitudes of marker 1 were significantly different from the maximum amplitudes (P<0.001, ANOVA with Tukey post hoc test) of the other markers and are therefore deemed unreliable and excluded from further analyses. The differences in maximum z-amplitude was significantly different between 8 and 10 phases for 60 BPM, 90 BPM and 100 BPM (P=.04, P=.002, P=.03). All

absolute differences were below 0.08 mm. Figure 4-6 illustrates an example of motions patterns for the 8 and 10 phases reconstructions and the sensor.

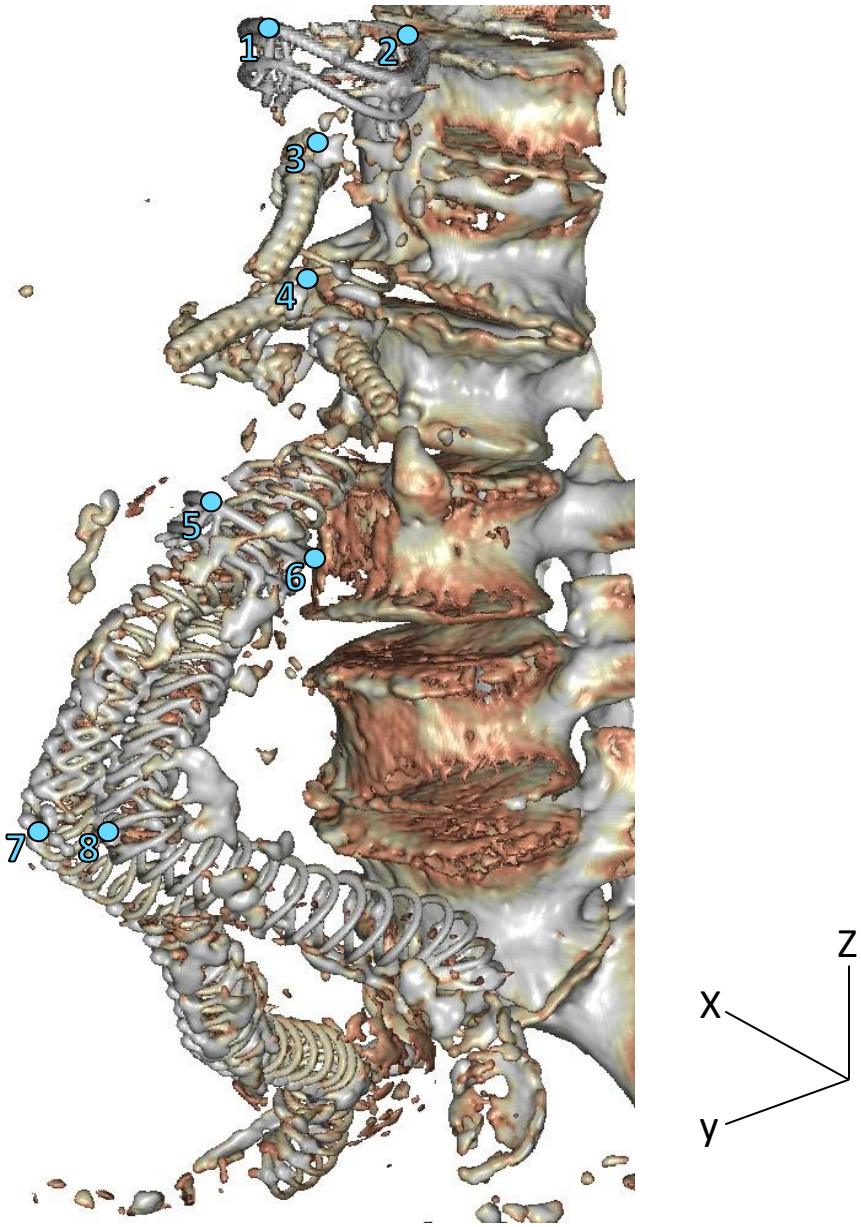

Figure 4-5. A 3D volume representation with the studied markers indicated.
The selected markers are presented and numbered in blue. The corresponding landmarks are: 1; ventral side of proximal ring FEVAR cuff, 2; dorsal side of proximal ring FEVAR cuff, 3; Origin of coeliac trunk branch, 4; Origin of the superior mesenteric artery branch, 5; ventral side of proximal ring of the main body, 6; dorsal side of the proximal ring of the main body, 7; Curve right iliac component. 8; Curve left iliac component.

Table 4-1 Maximum motion pattern amplitudes

	50 BPM		60 BPM		70 BPM		80 BPM		90 BPM		100 BPM		Sinus 50 BPM		Sinus 75 BPM	
	8	10	8	10	8	10	8	10	8	10	8	10	8	10	8	10
Marker 1	*0.90*	*0.96*	*0.86*	*0.82*	*1.04*	*0.97*	*1.26*	*1.24*	*1.08*	*1.10*	*1.10*	*1.04*	*1.41*	*1.34*	*1.43*	*1.44*
Marker 2	1.22	1.22	1.08	1.07	1.20	1.19	1.26	1.30	1.27	1.31	1.36	1.26	1.32	1.35	1.41	1.42
Marker 3	1.28	1.30	1.09	1.08	1.24	1.24	1.29	1.33	1.24	1.29	1.39	1.28	1.30	1.34	1.49	1.50
Marker 4	1.28	1.29	1.08	1.06	1.24	1.23	1.31	1.29	1.25	1.29	1.32	1.24	1.45	1.45	1.43	1.42
Marker 5	1.22	1.27	1.16	1.13	1.29	1.30	1.35	1.33	1.17	1.20	1.35	1.33	1.37	1.37	1.44	1.44
Difference	-0.02 ± 0.02		0.02 ± 0.01		0.00 ± 0.01		-0.01 ± 0.03		-0.04 ± 0.01		0.08 ± 0.04		0.00 ±0.05		0.00 ± 0.01	
Difference (%)	-2.2 ± 2.1		2.0 ± 1.2		1.3 ± 2.5		-0.3 ± 2.5		-2.9 ± 0.9		5.5 ± 2.6		0.0 ± 5.5		-0.3 ± 1.5	
P-value	.16		**.04**		.64		.60		**.002**		**.03**		1.000		.39	

Maximum motion pattern amplitudes are shown for the z-direction of marker per heartrate for the 8 and 10 phases ECG-gated CT reconstructions. Amplitudes are presented in millimeters (mm). Differences between 8 and 10 phases (defined as 8-10) are presented as mean ± SD and as percentage with regard to the mean of the 8 phases reconstruction amplitudes. For 50-100 BPM an aortic pressure profile wave was used as input. For sinus 50-75 BPM a sinusoidal wave was used as input. Marker 1 (grey) was excluded from analyses. Markers were selected at the following locations: Marker 1 was selected at the top of the longest leg of the endograft, marker 2 was selected at the top of the shortest leg, marker 3 and marker 4 were selected on the middle of the ventral (3) and dorsal(4) side the main body and marker 5 was selected at the end of the endograft. BPM, beats per minute; ECG, electrocardiogram; CT, computed tomography.

Table 4-2 Maximum motion pattern amplitudes (3D movements)

	60 BPM						70 BPM					
	X		Y		Z		X		Y		Z	
	8	10	8	10	8	10	8	10	8	10	8	10
Marker 1	*0.13*	*0.10*	*0.22*	*0.24*	*0.92*	*0.83*	*0.12*	*0.10*	*0.23*	*0.26*	*0.86*	*0.88*
Marker 2	0.09	0.09	0.13	0.16	1.31	1.35	0.10	0.10	0.21	0.21	1.35	1.33
Marker 3	0.08	0.11	0.13	0.16	1.29	1.33	0.10	0.09	0.19	0.19	1.31	1.29
Marker 4	0.07	0.09	0.13	0.16	1.25	1.24	0.10	0.11	0.18	0.18	1.21	1.23
Marker 5	0.09	0.16	0.13	0.08	1.40	1.42	0.11	0.17	0.10	0.14	1.31	1.31
Difference	-0.03 ± 0.03		-0.01 ± 0.04		-0.02 ± 0.02		-0.02 ± 0.03		-0.01 ± 0.02		0.00 ± 0.02	
Difference (%)	-36.0 ± 35.3		-7.6 ± 30.5		-1.7 ± 1.8		-14.8 ± 30.6		-5.8 ± 11.7		0.4 ± 1.5	
P-value	.13		.65		.15		.41		.39		.64	

The linear actuator was placed under a slope and diagonally to induce 3D movements. Maximum motion pattern amplitudes are shown for the x-, y- and z-direction of marker 1-5 per heartrate for the 8 and 10 phases ECG-gated CT reconstructions. Amplitudes are presented in millimeters (mm). Differences between 8 and 10 phases (defined as 8 minus 10) are presented as mean ± SD and as percentage with regard to the mean of the 8 phase reconstruction amplitudes. Marker 1 (grey) was excluded from analyses. Marker 1 was selected at the top of the longest leg of the endograft, marker 2 was selected at the top of the shortest leg, marker 3 and marker 4 were selected on the middle of the ventral (3) and dorsal(4) side the main body and marker 5 was selected at the end of the endograft. BPM, beats per minute; ECG, electrocardiogram; CT, computed tomography.

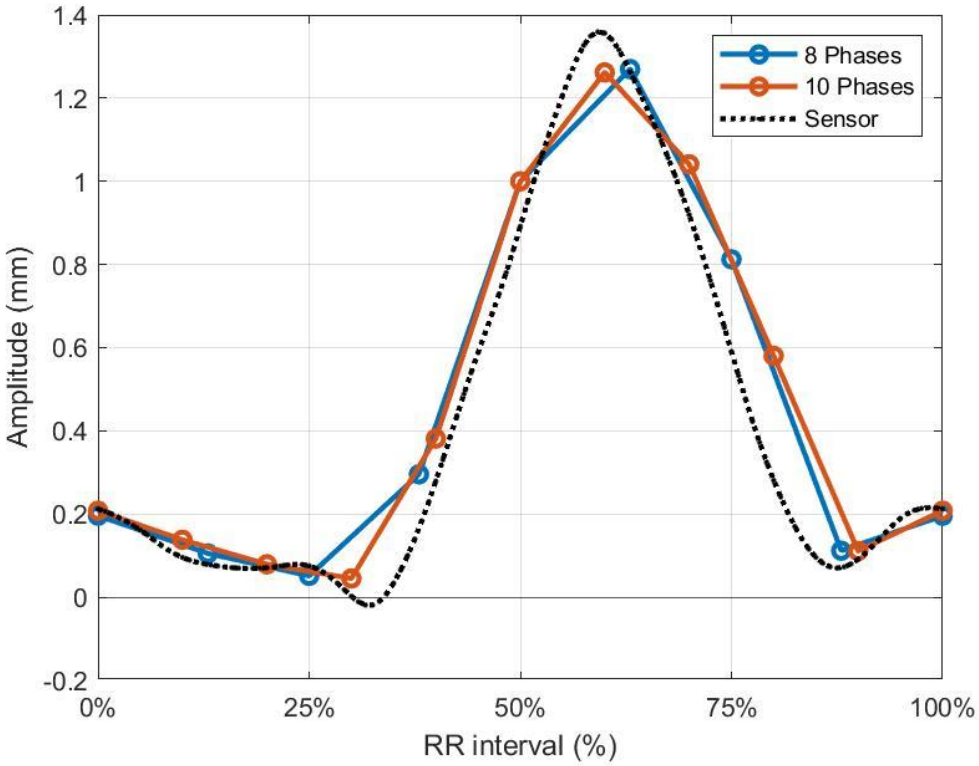

Figure 4-6 Example of displacement motion patterns of the 8 (blue line) and 10 (orange line) phases reconstructions compared to the sensor movement (black dashed line) during one cardiac cycle *The example represents the displacement of marker 2 during a heartrate of 50 beats per minute. Marker 2 was selected at the top of the shortest leg of the endograft. RR interval, heart rate.*

Pathlengths

Table 4-3 shows the pathlengths per measurement for each marker. The pathlengths of marker 1 were statistically different (*P*<.001, ANOVA with Tukey post hoc test) from the pathlengths of the other markers marker and are therefore deemed unreliable and excluded from further analyses. The differences in 8 and 10 phases reconstructions between the other selected markers were not significant (*P*=.30 to .48). The pathlengths of the 8 and 10 phases reconstructions were significantly different for 70 BPM, 90 BPM and 3D measurement 60 BPM (*P*=.003, *P*=.003, *P*=.022). The 8 phases pathlengths were higher for 70 BPM, while the 10 phases reconstruction was higher in at 90 BPM and 3D 60 BPM. The observed differences were <0.08 mm.

	Pathlength sensor (mm)	Pathlength 8 phases reconstruction (mm)	Pathlength 10 phases reconstruction (mm)
50 BPM	3.07	2.63 (2.60 2.72)	2.71 (2.63 2.79)
60 BPM	3.10	2.27 (2.18 2.44)	2.24 (2.12 2.41)
70 BPM	3.11	2.52 (2.46 2.61)	2.50 (2.44 2.60)
80 BPM	3.11	2.65 (2.52 2.84)	2.79 (2.77 2.82)

90 BPM	3.08	2.48 (2.34 2.57)	2.54 (2.40 2.62)
100 BPM	3.06	2.71 (2.63 2.77)	2.58 (2.47 2.72)
Sinus 50 BPM	2.86	2.74 (2.60 2.90)	2.74 (2.68 2.90)
Sinus 75 BPM	2.86	2.88 (2.82 2.98)	2.88 (2.83 2.99)
Differences aorta pressures			
	Sensor vs. 8 phases	**Sensor vs. 10 phases**	**8 phases vs. 10 phases**
Difference	0.55 ± 0.17	0.53 ± 0.20	-0.02 ± 0.1
Difference (%)	17.6 ± 5.5	17.1 ± 6.3	-0.54 ± 3.1
P-value	**0.001**	**0.001**	0.69

Table 4-4 shows the pathlengths measured by the Hall sensor. The pathlengths measured by the sensor were significantly higher (*P*=.001) than the pathlengths measured by the 8 and 10 phases reconstructions for the aortic pressure wave. The pathlengths of the 8 and 10 phases reconstructions were not significantly different (*P*=.69) from each other. The pathlengths of the sinus waves measured by the sensor were however not statistically different (*P*=0.60) from 8 and 10 phases reconstructions.

Table 4-3. Pathlengths of the 8 and 10 phases ECG-gated reconstructions per marker

	50 BPM		60 BPM		70 BPM		80 BPM		90B PM		100 BPM		60 BPM (3D)		70 BPM (3D)		Sinus 50 BPM		Sinus 75 BPM	
Phases	**8**	**10**	**8**	**10**	**8**	**10**	**8**	**10**	**8**	**10**	**8**	**10**	**8**	**10**	**8**	**10**	**8**	**10**	**8**	**10**
Marker 1	*1.84*	*2.02*	*1.77*	*1.71*	*2.16*	*1.97*	*2.54*	*2.54*	*2.19*	*2.20*	*2.26*	*2.10*	*2.08*	*1.94*	*2.00*	*2.07*	*2.48*	*2.20*	*2.47*	*2.41*
Marker 2	2.60	2.63	2.22	2.21	2.46	2.44	2.52	2.78	2.57	2.62	2.73	2.56	2.77	2.88	2.88	2.89	2.81	2.68	2.86	2.87
Marker 3	2.72	2.79	2.23	2.23	2.50	2.48	2.57	2.82	2.49	2.58	2.77	2.57	2.75	2.84	2.77	2.80	2.64	2.70	2.82	2.83
Marker 4	2.69	2.73	2.18	2.12	2.49	2.48	2.66	2.80	2.50	2.57	2.63	2.47	2.62	2.69	2.58	2.71	2.60	2.69	2.98	2.99
Marker 5	2.49	2.70	2.44	2.41	2.61	2.60	2.84	2.77	2.34	2.40	2.71	2.72	2.98	3.01	2.83	2.98	2.90	2.90	2.85	2.84
Difference	-0.09 ± 0.09		0.03 ± 0.03		0.01 ± 0.00		-0.15 ± 0.15		-0.07 ± 0.02		0.13 ± 0.10		-0.07 ± 0.03		-0.08 ± 0.07		0.00 ± 0.10		-0.01 ± 0.01	
Difference (%)	-3.2 ± 3.4		1.2 ± 1.2		0.6 ± 0.1		-5.5 ± 5.8		-2.9 ± 0.6		4.7 ± 3.6		-2.7 ± 1.2		-2.9 ± 2.5		-0.2 ± 3.6		-0.2 ± 0.3	
P-value	.14		.14		**.003**		.15		**.003**		.080		**.022**		.11		.93		.39	

Pathlengths of marker 1-5 per heartrate are given for the 8 phases reconstructions and 10 phases reconstructions. Pathlengths are presented in millimeters (mm). The pathlength was defined as the sum distances between subsequent locations of each marker during cardiac cycle. Differences between 8 and 10 phases (defined as 8-10) are presented as mean ± SD and as percentage with regard to the mean of the amplitudes of the 8 phase reconstructions. For 50-100 BPM an aortic pressure profile wave was used as input. For 60-70 BPM (3D) the linear actuator was placed on a slope and diagonally to induce 3D movements. For sinus 50-75 BPM a sinusoidal wave was used as input. Marker 1 (grey) was excluded from analyses. Marker 1 was selected at the top of the longest leg of the endograft, marker 2 was selected at the top of the shortest leg, marker 3 and marker 4 were selected on the middle of the ventral (3) and dorsal(4) side the main body and marker 5 was selected at the end of the endograft. BPM, beats per minute.

Table 4-4. Sensor pathlengths compared with the pathlengths of the 8 and 10 phases ECG-gated reconstructions

	Pathlength sensor (mm)	Pathlength 8 phases reconstruction (mm)	Pathlength 10 phases reconstruction (mm)
50 BPM	3.07	2.63 (2.60 2.72)	2.71 (2.63 2.79)
60 BPM	3.10	2.27 (2.18 2.44)	2.24 (2.12 2.41)
70 BPM	3.11	2.52 (2.46 2.61)	2.50 (2.44 2.60)
80 BPM	3.11	2.65 (2.52 2.84)	2.79 (2.77 2.82)
90 BPM	3.08	2.48 (2.34 2.57)	2.54 (2.40 2.62)
100 BPM	3.06	2.71 (2.63 2.77)	2.58 (2.47 2.72)
Sinus 50 BPM	2.86	2.74 (2.60 2.90)	2.74 (2.68 2.90)
Sinus 75 BPM	2.86	2.88 (2.82 2.98)	2.88 (2.83 2.99)
Differences aorta pressures			
	Sensor vs. 8 phases	**Sensor vs. 10 phases**	**8 phases vs. 10 phases**
Difference	0.55 ± 0.17	0.53 ± 0.20	-0.02 ± 0.1
Difference (%)	17.6 ± 5.5	17.1 ± 6.3	-0.54 ± 3.1
P-value	**0.001**	**0.001**	0.69

The pathlengths of the 8 and 10 phases reconstructions are presented as the mean (min max) value of the pathlengths measured in marker 2-5. Differences are presented as mean ± SD and as percentage with regard to the mean of the 8 phase reconstruction amplitudes. For 50-100 BPM an aortic pressure profile wave was used as input. For sinus 50-75 BPM a sinusoidal wave was used as input. BPM, beats per minute; ECG, electrocardiogram; CT, computed tomography.

Simulation of possible start points

The negative mean values in Table 4-5 implicate that on average the pathlengths of the 10 phases reconstructions were longer. However, the positive values in the maximum differences show that at some starting points the pathlengths of 8 phases reconstructions were higher. Based on the start location either the 8 phases reconstruction can show a longer pathlength than the 10 phases reconstruction with a maximum of 0.17 mm difference, or the 10 phases pathlength can show a longer pathlength with a maximum of 0.56 mm difference.

Table 4-5 Pathlengths differences of simulated 8 and 10 phases reconstructions

	50 BPM	60 BPM	70 BPM	80 BPM	90 BPM	100 BPM
Mean (mm)	-0.20 (-8.4)	-0.17 (-7.2)	-0.20 (-8.6)	-0.16 (-6.5)	-0.16 (-6.3)	-0.15 (-5.8)
Min (mm)	-0.56 (-27.4)	-0.50 (-22.6)	-0.53 (-25.2)	-0.48 (-21.1)	-0.50 (-21.6)	-0.44 (-18.6)
Max (mm)	0.10 (3.8)	0.15 (5.9)	0.13 (5.0)	0.17 (5.9)	0.16 (5.9)	0.14 (5.3)

At each possible start point the difference in pathlengths between the 8 and 10 phases reconstructions was calculated by subtracting the 8 phases pathlengths from the 10 phases pathlengths. Differences are presented per heartrate as mean, minimum (min) and maximum (max) with the percentage with regard to the 8 phases reconstructions. BPM, beats per minute

4.3.2 *Explorative patient study*

The observed motion amplitudes in x-, y-, and z-directions were all below 1 mm, see Figure 4-7. Largest movement was found in the Y-direction. Hardly any movement is observed at the dorsal side of the proximal ring of the cuff (marker 2). The maximum amplitudes are shown in Table 4-6. The maximum amplitudes between the 8 and 10 phases scan were not significantly different for all directions (*P*=0.16,

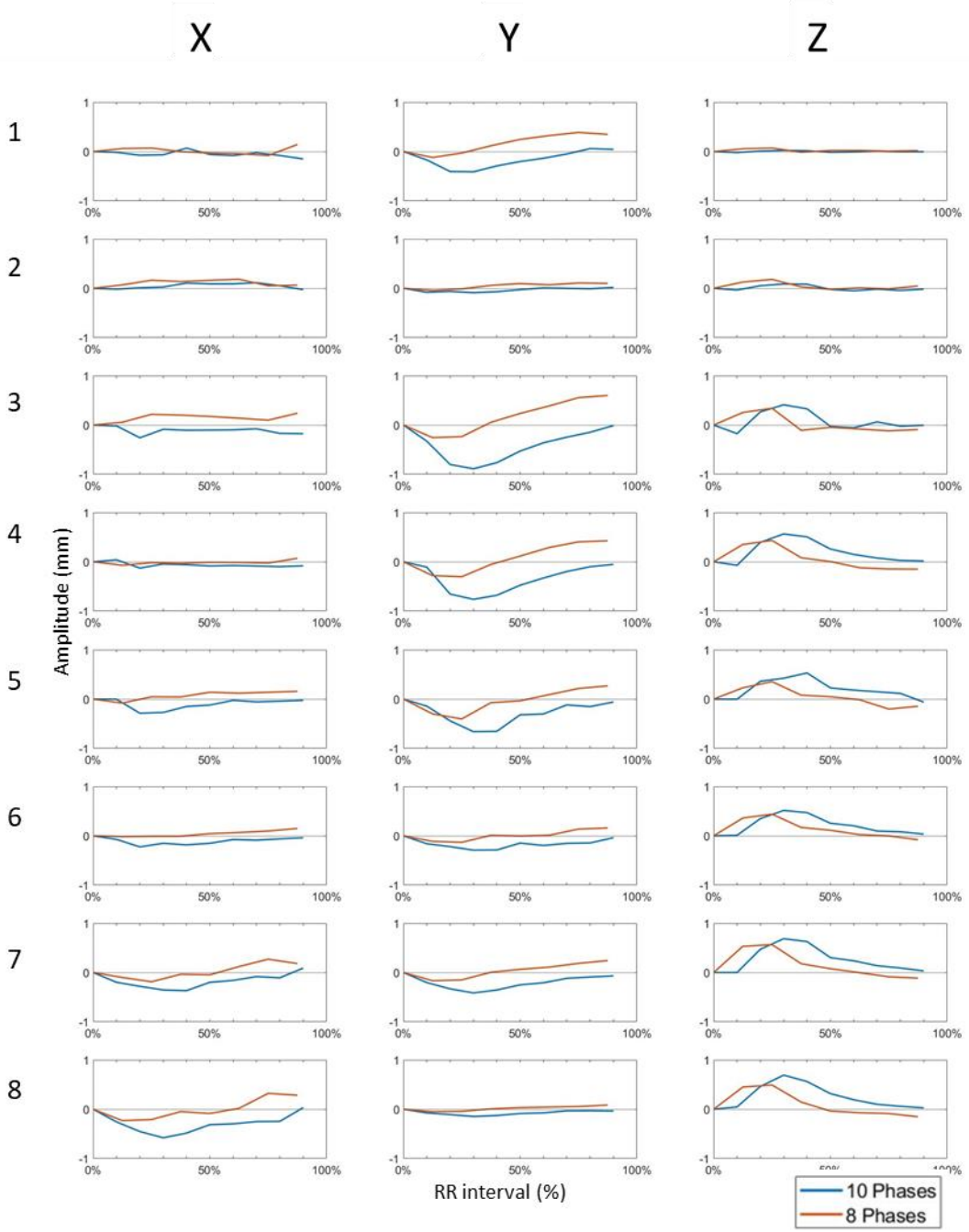

Figure 4-7 The displacement in x-, y- and z-direction per marker *The corresponding landmarks to the markers are: 1; ventral side of proximal ring FEVAR cuff, 2; dorsal side of proximal ring FEVAR cuff, 3; Origin of coeliac trunk branch, 4; Origin of the superior mesenteric artery branch, 5; ventral side of proximal ring of the main body, 6; dorsal side of the proximal ring of the main body, 7; Ventral curve right iliac component. 8; Ventral curve left iliac component.*

P=.89, *P*=.38). Table 4-7 shows the pathlengths per marker. The pathlengths of the markers in the 8 phases reconstruction were not statistically different from the markers in the 10 phases reconstruction (*P*=.15).

Table 4-6 Maximal amplitudes in x-,y-, and z-direction per marker

	X (mm)		Y (mm)		Z (mm)	
	8 phases scan	10 phases scan	8 phases scan	10 phases scan	8 phases scan	10 phases scan
Ventral side proximal ring cuff	0.22	0.22	0.51	0.47	0.09	0.04
Dorsal side proximal ring cuff	0.18	0.14	0.15	0.11	0.20	0.14
Origin of coeliac trunk branch	0.24	0.26	0.85	0.89	0.46	0.58
Origin of the superior mesenteric artery branch	0.14	0.17	0.73	0.76	0.58	0.64
Ventral side proximal ring main body	0.24	0.29	0.67	0.66	0.56	0.59
Dorsal side proximal ring main body	0.16	0.22	0.29	0.29	0.52	0.52
Curve right iliac component	0.46	0.46	0.41	0.41	0.68	0.69
Curve left iliac component	0.55	0.61	0.14	0.15	0.64	0.69
mean	0.28	0.30	0.47	0.47	0.47	0.49
Difference	-0.02 ± 0.04		0.00 ± 0.03		-0.02 ± 0.06	
Difference (%)	-7.2 ± 13.0		0.3 ± 6.2		-4.3 ± 12.8	
P-Value	.15		.89		.38	

Differences are presented as mean ± SD and as percentage with regard to the mean of the 8 phases reconstruction amplitudes.

Table 4-7 Pathlength per marker of the 8 and 10 phases reconstruction

	Pathlength 8 phases scan (mm)	Pathlength 10 phases scan (mm)
Ventral side proximal ring cuff	1.32	1.30
Dorsal side proximal ring cuff	0.88	0.70
Origin of coeliac trunk branch	2.42	2.69
Origin of the superior mesenteric artery branch	2.06	2.11
Ventral side proximal ring main body	1.92	2.17
Dorsal side proximal ring main body	1.40	1.50
Curve right iliac component	1.96	2.08
Curve left iliac component	2.04	2.11
mean	1.75	2.11
Difference	-0.08 ± 0.14	
Difference (%)	-4.7 ± 8.2	
P-value	.15	

Differences are presented as mean ± SD and as percentage with regard to the mean of the 8 phases reconstruction amplitudes.

4.4 Discussion

The in vitro experiment of this study showed a statistically significant difference between 8 and 10 phases reconstructions was found in maximum amplitude for 60 BPM, 90 BPM and 100 BPM and in pathlength for 70 BPM, 90 BPM and 3D measurement 60 BPM. The absolute mean difference was found to be <0.08 mm for the maximum amplitudes and for the pathlengths <0.08 mm which negligible as the current IBD study reported amplitudes with magnitudes of tenths of millimeters and pathlengths with magnitudes of millimeters. Moreover, the values are below the error value of 0.3 mm of the used software (49). Furthermore, the explorative patients study showed no significant difference between 8 and 10 phases reconstructions in amplitudes and pathlengths. The computer simulation showed that the pathlengths of the 10 phases reconstructions could be, at maximum, 0.56 mm higher than the pathlengths of the 8 phases reconstructions. This result is above the software error value, but below the pathlength differences found in the IBD study.

These protocols with a different amount of cardiac phases have not been compared before. Fundamental research was conducted by Klein et al (72). They found that a minimal number of phases is required to get overlap between subsequent phases and that a maximum amount of phases should be set to avoid more than 50% overlap. In their study they used a heartrate of 50 BPM which required a number of phases between 8 and 12. However, these conclusions cannot be applied to our in vitro study as they were performed on a Siemens Somatom 64-slice CT scanner, while the study for the in vitro study was

performed on a Philips Brilliance iCT 256. Each manufacturer applies proprietary optimizations and corrections to complex reconstruction algorithms also chosen by the manufacturer. Such details are not published. The explorative patient study did use a Siemens Somatom 64-slice CT scanner, but the results of Klein et al cannot be applied here either as the scan protocols differ in rotation time, collimation and reconstruction filter/kernel. Moreover, the heartrate of the patient in this study was unknown.

Results of marker 1 of the in vitro experiment were excluded as the amplitudes as well as the pathlengths were significantly different from the other markers. An explanation for this deviation is the location of the marker at the top of the scan. Presumably, this marker is out of view when moving. In future studies a larger margins around object of interest should be taken. Moreover, it is recommended not to choose markers that are located along the edges of the scan.

The observed pathlengths in the in vitro experiment ranged from to 2.18 to 3.01 mm. This corresponds to markers placed at the most dynamic points in the explorative patients study, like the origin of the celiac trunk branch that had a pathlength of 2.42-2.69mm. The ranges of the maximum amplitudes found in the in vitro study are quite high compared to the amplitudes measured in the patient study (1.07 to 1.37 mm vs 0.04 to 0.89 mm respectively). However, lower amplitudes would have led to lower pathlengths as the motion was only determined in one direction.

Although no difference was observed between the 8 phases and 10 phases pathlengths, these pathlengths were different from the sensor pathlengths (P=.001). This implies that 8 phases and 10 phases motion patterns were not a perfect representation of the real movement of the endograft which is also shown in Figure 4-6. However, the sensor pathlengths of the sinus functions were not statistically different from the pathlengths of the 8 phases and 10 phases reconstructions. This means that the unknown algorithm of the CT scanner is able to reconstruct movement according to a single frequency wave, but does not reconstruct movements according to waves consisting of more frequencies. This might be caused by the quick changes in the aorta pressure wave. Klein et al. showed that the pressure wave contained frequency up to up to 5 Hz (72). Follow-up research including sinusoidal waveform with higher frequencies is needed verify this statement.

Limitations

The potential instability of experimental set-up may be considered a limitation of the study. Although care was taken in transporting the linear actuator, the sensor showed an off-set after the measurements were performed. However, this offset did not affect our results as we only look at the relative movements, which could still be accurately measured by the sensor. Furthermore, the linear actuator was not synchronized with the ECG-phantom, leading to a random scanning start point in the continuous movement of the linear actuator. Several measurements were performed and none of them showed significant differences above 0.08 mm between the 8 and the 10 phases measurements. It is therefore unlikely that synchronization would induce significant differences between 8 and 10 phases reconstructions. Furthermore, a simulation was performed including alle possible start points based on the sensor data which did retrieve the movement accurately. This simulation was however an approximation of the CT reconstruction. A follow-up experiment including synchronization would be more accurate.

Another potential limitation in this study could be the movement of the linear actuator in one direction is. However, two additional measurements were performed with inducing a 3D measurement. Also, these measurements did not reveal any differences between the 8 and 10 phases pathlengths or amplitudes. The amplitudes in the x-direction were however quite small (<0.17 mm) implying that the diagonal placement of the linear actuator was modest. In follow-up research, more attention should be given on how the linear actuator is placed for the 3D measurements.

At last, the in vitro study was performed on one CT scan only. Therefore, it is uncertain if the same conclusions apply to other scanners. However, the patient study was performed on a different type of CT scanner than the in vitro experiment. The outcomes of the patient study did not result in significant differences between 8 phases and 10 phases scans as well.

Conclusion

This study revealed that 8 and 10 phases ECG-gated CT scans can be compared to each other when taking into account that the difference in reconstruction protocol can cause the 10 phases reconstructions to be 0.56 mm higher than the 8 phases reconstructions at maximum. Follow-up research would probable even reduce this difference.

5 General discussion and conclusion

This thesis focused on two main studies. The first main study focused on aortic remodeling after EVAR based on diameters and curvatures. However, the intra- and inter observer study in this thesis showed moderate agreement of curvature measurements between two observers. The limitations of this study prohibit a fair statement about the reliability of curvature as a whole. Nonetheless, this observer study does imply that the CLLs, the basis for curvature calculations, should be constructed with great care, which requires a detailed measurement protocol and an adequate training. As outliers occurred in measurements of both observers, both observers were not adequately trained. Moreover, the initial protocol used by observer 1 had ambiguous indications and was therefore subject to the observers interpretation. The curvature measurements performed on the Endurant cohort were not remeasured due to technical limitations and time limitations of this thesis. Therefore, the difference in remodeling between Anaconda and Endurant could not be examined based on curvature. Nevertheless, curvature seems to be a promising tool to define aortic remodeling in future studies as remodeling of the suprarenal and infrarenal aorta base on curvature was found related to patient outcome in previous literature (40,51,73).

The intra- and interobserver study found an excellent observer agreement for diameters lengths and angulation. Diameters could be measured with a median variability of ≤1 mm for intra and inter observer variability. Median neck length difference was found 0.0 for interobserver variability and 0.4 mm for intra observer variability. Alpha and beta angulation differed on average 2.0° and 4.5° for interobserver variability and 1.0° and 0.5° for intra observer variability, respectively. Therefore, the difference in aortic remodeling between the Anaconda and Endurant could be examined based on aortic neck diameters at different levels with regard to the lowest renal artery. The diameters measured in the Anaconda cohort did not change at any level, while the diameters measured in the Endurant cohort increased at all levels except at 30 mm above the baseline. These findings indicate that the Anaconda self-expandable rings may exert less forces on the aortic wall than the anchor pins of the Endurant endograft. The Endurant therefore induces advanced neck enlargement which had been reported in previously (65,66). However, this study included only the first postoperative CT scan, so it is unknown how these aorta's remodel over time. Moreover, comparison of remodeling after EVAR between Anaconda and Endurant was limited by the poor availability of data. Endurant measurements were performed for a different study purpose by a previous observer and were not adjusted for this thesis. Therefore, suboptimal levels of the aortic neck were examined as more levels distal to the baseline have been measured to examine the findings of Koenrades et al.(33). Other dimensional measurements could not be used to define remodeling as these were not measured postoperatively by the Endurant observer. Remodeling based on diameters only is quite modest as remodeling could have been expressed in postoperative changes of lengths, angulation, maximum aneurysm diameter and curvature as well.

Aortic remodeling can also be expressed as the change in postoperative motion patterns using ECG-gated CTA scans. In this thesis, an in vitro experiment was performed to compare motion calculations between 10 and 8 phases reconstructions of ECG-gated scans. The results revealed that the only significant differences between the 8 and 10 phases reconstructions were below the error value of the measurement software. The linear actuator was not synchronized with the CT scanner which might be considered a limitation of this study, because the CT-scanners started at a random point in the movement. A computer simulation was performed to assess the effect of different starting points of the blood pressure curve on the resulting pathlengths. As upper limit, the pathlengths of the 10 phases reconstructions were 0.56 mm larger than the pathlengths of the 8 phases reconstructions. Therefore, when comparing pathlengths in CT scans with 8 and 10 phases reconstructions, differences of 0.56 mm and less could be caused by the phase difference. However, the real threshold is expected to be lower. The threshold of 0.56 mm was

found at 50 BPM, so there were 120 possible start points of which one resulted in a pathlength difference of 0.56 mm. Therefore, the change that this sample is chosen as starting sample is 1 out of 120. However, this simulation was a simplification of the unknown reconstruction algorithms of the CT-scanner. Therefore, it is recommended to repeat this study when the technical limitation is resolved and the linear actuator can be synchronized with the CT scanner. However, in this study, several measurements were performed in vitro as well as in vivo which all did not result in a clinically relevant difference between the 8 and 10 phases reconstructions. Therefore, it is not expected that synchronization will reveal a significant difference.

Conclusion

Aortic remodeling based on curvature could not be determined in this thesis due to moderate observer agreement, although dimensional measurements showed excellent observer agreement. When performing an adequate intra- and inter observer study on aortic curvature, remodeling based on curvature can be examined in future research. Aortic remodeling based on aortic supra-, juxta- and infrarenal neck diameters measured on the preoperative and first postoperative CT scan revealed that the Anaconda endograft did not change while infrarenal neck enlargement was found in the Endurant endografts. Future research should include more follow-up scans, more infrarenal diameters and include patient outcome to examine the relation between aortic remodeling and possible complications.

When examining the dynamic aortic remodeling on ECG-gated CTA scans based on motion patterns and pathlengths, 8 phases reconstructions can be compared with 10 phases reconstructions when taking into account that the difference in reconstruction protocol can cause the 10 phases reconstructions to be at maximum 0.56 mm higher than the 8 phases reconstructions.

6 Future perspectives and recommendations

The goal of research into remodeling after EVAR is to identify causes of EVAR-related complications in order to overcome these complications and design durable endografts. Moreover, knowledge on aortic remodeling could be used to design endografts for patients with a more severe angulated anatomy. Despite the remodeling after EVAR could not be determined based on curvature in this thesis, curvature could still be a usable tool to define the aortic remodeling. Nevertheless, a well-designed intra- and interobserver study should first be conducted. Observers should have the same background and should be trained on how to accurately perform the measurements by an expert. The measurements should be performed according to an unambiguous protocol for which the measurement protocol in Appendix A can serve as basis. This protocol is based on measurements in 3mensio, but other measurement software should be included as well. After the intra- and interobserver variability is determined the measurements on the Anaconda and Endurant pre- and postoperative should be performed by the same observer(s) to define the remodeling by both endografts. Moreover, follow-up scans can be included to define the aortic remodeling over time. When defining the remodeling in curvature, also matching preoperative characteristics should be taken into account such as curvature. More remodeling is expected in more angulated segments. Therefore, cohorts should be matched on preoperative curvature. After the aortic remodeling is determined, the relation with patient outcome can be examined and consequently, preoperative risks might be identified.

In this thesis an in vitro set-up was used to determine to what extent an 8 phases reconstruction or a 10 phases can cause a difference in motion patterns and pathlengths. Due to technical limitations, the linear actuator could not be synchronized with the CT scanner. The ECG-phantom that triggered the CT scanner could not create a pulse of 5 Volt which was needed to trigger the waveform generator that excited the linear actuator. Currently, an in-house built open-loop amplifier has been manufactured that is able to amplify the ECG-pulse and therefore trigger the waveform generator. The measurements can therefore be repeated with synchronization of the linear actuator and the CT scanner. Each manufacturer applies proprietary optimizations and corrections to complex reconstruction algorithms also chosen by the manufacturer. Such details are not published. It is therefore recommend to repeat these measurements on a different type of CT scanner to assess whether the results apply to other CT scanners. The results of this study can be used for studies comparing aortic motions ECG-gated CTA scans on scans with 8 and 10 phases reconstructions, as observed in the current IBD study. Knowledge of the difference in motion characteristics and geometries can help identify causes of endograft failure and consequently improve future designs, leading to more durable endografts.

References

1. Aggarwal S, Qamar A, Sharma V, Sharma A. Abdominal aortic aneurysm: A comprehensive review. Exp Clin Cardiol. 2011;16(1):11–5.

2. Li X, Zhao G, Zhang J, Duan Z, Xin S. Prevalence and Trends of the Abdominal Aortic Aneurysms Epidemic in General Population - A Meta-Analysis. PLoS ONE [Internet]. 2013 Dec 2 [cited 2020 Sep 4];8(12). Available from: https://www.ncbi.nlm.nih.gov/pmc/articles/PMC3846841/

3. Ullery BW, Hallett RL, Fleischmann D. Epidemiology and contemporary management of abdominal aortic aneurysms. Abdom Radiol N Y. 2018;43(5):1032–43.

4. Crawford ES, Beckett WC, Greer MS. Juxtarenal infrarenal abdominal aortic aneurysm. Special diagnostic and therapeutic considerations. Ann Surg. 1986 Jun;203(6):661–70.

5. Wanhainen A, Verzini F, Van Herzeele I, Allaire E, Bown M, Cohnert T, et al. Editor's Choice - European Society for Vascular Surgery (ESVS) 2019 Clinical Practice Guidelines on the Management of Abdominal Aorto-iliac Artery Aneurysms. Eur J Vasc Endovasc Surg Off J Eur Soc Vasc Surg. 2019 Jan;57(1):8–93.

6. Lee A, Dake MD. Abdominal and Thoracic Aortic Aneurysms. In: Keefe NA, Haskal ZJ, Park AW, Angle JF, editors. IR Playbook: A Comprehensive Introduction to Interventional Radiology [Internet]. Cham: Springer International Publishing; 2018 [cited 2020 Sep 28]. p. 197–207. Available from: https://doi.org/10.1007/978-3-319-71300-7_17

7. Sweeting MJ, Thompson SG, Brown LC, Powell JT, RESCAN collaborators. Meta-analysis of individual patient data to examine factors affecting growth and rupture of small abdominal aortic aneurysms. Br J Surg. 2012 May;99(5):655–65.

8. Reimerink JJ, van der Laan MJ, Koelemay MJ, Balm R, Legemate DA. Systematic review and meta-analysis of population-based mortality from ruptured abdominal aortic aneurysm. Br J Surg. 2013 Oct;100(11):1405–13.

9. Livesay JJ, Messner GN, Vaughn WK. Milestones in Treatment of Aortic Aneurysm. Tex Heart Inst J. 2005;32(2):130–4.

10. Lederle FA, Freischlag JA, Kyriakides TC, Padberg FT, Matsumura JS, Kohler TR, et al. Outcomes following endovascular vs open repair of abdominal aortic aneurysm: a randomized trial. JAMA. 2009 Oct 14;302(14):1535–42.

11. Greenhalgh R. Comparison of endovascular aneurysm repair with open repair in patients with abdominal aortic aneurysm (EVAR trial 1), 30-day operative mortality results: randomised controlled trial. The Lancet. 2004 Sep 4;364(9437):843–8.

12. Antoniou GA, Antoniou SA, Torella F. Editor's Choice – Endovascular vs. Open Repair for Abdominal Aortic Aneurysm: Systematic Review and Meta-analysis of Updated Peri-operative and Long Term Data of Randomised Controlled Trials. Eur J Vasc Endovasc Surg. 2020 Mar;59(3):385–97.

13. Ricco J-B, Cau J, Biancari F, Desvergnes M, Lefort N, Belmonte R, et al. Outcome After Open and Laparoscopic Aortic Surgery in Matched Cohorts Using Propensity Score Matching. Eur J Vasc Endovasc Surg Off J Eur Soc Vasc Surg. 2016 Aug;52(2):179–88.

14. Volodos' NL, Karpovich IP, Shekhanin VE, Troian VI, Iakovenko LF. [A case of distant transfemoral endoprosthesis of the thoracic artery using a self-fixing synthetic prosthesis in traumatic aneurysm]. Grud Khirurgiia Mosc Russ. 1988 Dec;(6):84–6.

15. Lee WA, Brown MP, Nelson PR, Huber TS. Total percutaneous access for endovascular aortic aneurysm repair ("Preclose" technique). J Vasc Surg. 2007 Jun;45(6):1095–101.

16. Lederle FA, Kyriakides TC, Stroupe KT, Freischlag JA, Padberg FT, Matsumura JS, et al. Open versus Endovascular Repair of Abdominal Aortic Aneurysm. N Engl J Med. 2019 May 30;380(22):2126–35.

17. Blankensteijn JD, De Jong SECA, Prinssen M, Van Der Ham AC, Buth J, Van Sterkenburg SMM, et al. Two-year outcomes after conventional or endovascular repair of abdominal aortic aneurysms. N Engl J Med. 2005;352(23):2398–405.

18. Becquemin J-P, Pillet J-C, Lescalie F, Sapoval M, Goueffic Y, Lermusiaux P, et al. A randomized controlled trial of endovascular aneurysm repair versus open surgery for abdominal aortic aneurysms in low- to moderate-risk patients. J Vasc Surg. 2011;53(5):1167-1173.e1.

19. Brown LC, Powell JT, Thompson SG, Epstein DM, Sculpher MJ, Greenhalgh RM. The UK EndoVascular Aneurysm Repair (EVAR) trials: randomised trials of EVAR versus standard therapy. Health Technol Assess [Internet]. 2012 Mar 5 [cited 2020 Sep 7];16(9). Available from: https://www.journalslibrary.nihr.ac.uk/hta/hta16090/#/abstract

20. Patel R, Sweeting MJ, Powell JT, Greenhalgh RM. Endovascular versus open repair of abdominal aortic aneurysm in 15-years' follow-up of the UK endovascular aneurysm repair trial 1 (EVAR trial 1): a randomised controlled trial. The Lancet. 2016 Nov 12;388(10058):2366–74.

21. Kim HO, Yim NY, Kim JK, Kang YJ, Lee BC. Endovascular Aneurysm Repair for Abdominal Aortic Aneurysm: A Comprehensive Review. Korean J Radiol. 2019 Aug;20(8):1247–65.

22. White SB, Stavropoulos SW. Management of Endoleaks following Endovascular Aneurysm Repair. Semin Interv Radiol. 2009 Mar;26(1):33–8.

23. Silverberg D, Baril DT, Ellozy SH, Carroccio A, Greyrose SE, Lookstein RA, et al. An 8-year experience with type II endoleaks: Natural history suggests selective intervention is a safe approach. J Vasc Surg. 2006 Sep;44(3):453–9.

24. Cerna M, Köcher M, Utikal P, Bachleda P. Endotension after endovascular treatment of abdominal aortic aneurysm: Percutaneous treatment. J Vasc Surg. 2009 Sep 1;50(3):648–51.

25. Daye D, Walker TG. Complications of endovascular aneurysm repair of the thoracic and abdominal aorta: evaluation and management. Cardiovasc Diagn Ther. 2018 Apr;8(Suppl 1):S138–56.

26. Bley T, Roos J. Pre- and Post-aortic Endovascular Interventions: What a Radiologist Needs to Know. In: Hodler J, Kubik-Huch RA, von Schulthess GK, editors. Diseases of the Chest, Breast, Heart and

Vessels 2019-2022: Diagnostic and Interventional Imaging [Internet]. Cham: Springer International Publishing; 2019 [cited 2020 Oct 1]. p. 215–22. (IDKD Springer Series). Available from: https://doi.org/10.1007/978-3-030-11149-6_19

27. Carpenter JP, Baum RA, Barker CF, Golden MA, Mitchell ME, Velazquez OC, et al. Impact of exclusion criteria on patient selection for endovascular abdominal aortic aneurysm repair. J Vasc Surg. 2001 Dec 1;34(6):1050–4.

28. Schanzer Andres, Greenberg Roy K., Hevelone Nathanael, Robinson William P., Eslami Mohammad H., Goldberg Robert J., et al. Predictors of Abdominal Aortic Aneurysm Sac Enlargement After Endovascular Repair. Circulation. 2011 Jun 21;123(24):2848–55.

29. Rödel SGJ, Zeebregts CJ, Huisman AB, Geelkerken RH. Results of the Anaconda endovascular graft in abdominal aortic aneurysm with a severe angulated infrarenal neck. J Vasc Surg. 2014 Jun 1;59(6):1495-1501.e1.

30. Freyrie A, Testi G, Faggioli G, Gargiulo M, Giovanetti F, Serra C, et al. Ring-stents supported infrarenal aortic endograft fits well in abdominal aortic aneurysms with tortuous anatomy. J Cardiovasc Surg (Torino). 2010;

31. Bungay P. The use of the Anaconda™ stent graft for abdominal aortic aneurysms. J Cardiovasc Surg (Torino). 2012 Oct;53(5):571–7.

32. Rödel SGJ, Zeebregts CJ, Meerwaldt R, van der Palen J, Geelkerken RH. Incidence and Treatment of Limb Occlusion of the Anaconda Endograft After Endovascular Aneurysm Repair. J Endovasc Ther Off J Int Soc Endovasc Spec. 2019;26(1):113–20.

33. Simmering JA, Geelkerken RH, Slump CH, Koenrades MA. Geometrical changes in Anaconda endograft limbs after endovascular aneurysm repair: A potential predictor for limb occlusion. Semin Vasc Surg. 2020 Mar 1;32(3):94–105.

34. Pecoraro F, Corte G, Dinoto E, Badalamenti G, Bruno S, Bajardi G. Clinical outcomes of Endurant II stent-graft for infrarenal aortic aneurysm repair: comparison of on-label versus off-label use. Diagn Interv Radiol. 2016 Sep;22(5):450–4.

35. van Keulen JW, de Vries J-PPM, Dekker H, Gonçalves FB, Moll FL, Verhagen HJ, et al. One-year multicenter results of 100 abdominal aortic aneurysm patients treated with the Endurant stent graft. J Vasc Surg. 2011 Sep;54(3):609–15.

36. Bastos Goncalves F, Hoeks SE, Teijink JA, Moll FL, Castro JA, Stolker RJ, et al. Risk Factors for Proximal Neck Complications After Endovascular Aneurysm Repair Using the Endurant Stentgraft. Eur J Vasc Endovasc Surg. 2015 Feb 1;49(2):156–62.

37. Oliveira-Pinto J, Oliveira NFG, Bastos-Gonçalves FM, Hoeks S, Rijn MJV, Raa ST, et al. Long-term results after standard endovascular aneurysm repair with the Endurant and Excluder stent grafts. J Vasc Surg. 2020;71(1):64–74.

38. Anaconda™ Instructions for Use [Internet]. Terumo-Aortic; [cited 2020 Oct 16]. Available from: https://terumoaortic.com/products/anaconda/

39. Endurant™ IIs Instructions for use. Medtronic;

40. Schuurmann RCL, van Noort K, Overeem SP, Ouriel K, Jordan WD, Muhs BE, et al. Aortic Curvature Is a Predictor of Late Type Ia Endoleak and Migration After Endovascular Aneurysm Repair. J Endovasc Ther Off J Int Soc Endovasc Spec. 2017;24(3):411–7.

41. Schuurmann RCL, Kuster L, Slump CH, Vahl A, van den Heuvel DAF, Ouriel K, et al. Aortic Curvature Instead of Angulation Allows Improved Estimation of the True Aorto-iliac Trajectory. Eur J Vasc Endovasc Surg. 2016 Feb 1;51(2):216–24.

42. Schuurmann RCL, Ouriel K, Muhs BE, Jordan WD, Ouriel RL, Boersen JT, et al. Aortic curvature as a predictor of intraoperative type Ia endoleak. J Vasc Surg. 2016 Mar 1;63(3):596–602.

43. Tasso P, Raptis A, Matsagkas M, Lodi Rizzini M, Gallo D, Xenos M, et al. Abdominal aortic aneurysm endovascular repair: profiling post-implantation morphometry and hemodynamics with image-based computational fluid dynamics. J Biomech Eng. 2018 May 23;

44. Figueroa CA, Taylor CA, Yeh V, Chiou AJ, Zarins CK. Effect of curvature on displacement forces acting on aortic endografts: a 3-dimensional computational analysis. J Endovasc Ther Off J Int Soc Endovasc Spec. 2009 Jun;16(3):284–94.

45. Langs G, Paragios N, Desgranges P, Rahmouni A, Kobeiter H. Learning deformation and structure simultaneously: In situ endograft deformation analysis. Med Image Anal. 2011 Feb 1;15(1):12–21.

46. de Beaufort HWL, Nauta FJH, Conti M, Cellitti E, Trentin C, Faggiano E, et al. Extensibility and Distensibility of the Thoracic Aorta in Patients with Aneurysm. Eur J Vasc Endovasc Surg Off J Eur Soc Vasc Surg. 2017 Feb;53(2):199–205.

47. Klein A, Renema W, Oostveen L, schultze kool L, Slump C, Hu X, et al. A segmentation method for stentgrafts in the abdominal aorta from ECG-gated CTA data - art. no. 69160R. 2008 Mar 6;6916.

48. Klein A, van der Vliet JA, Oostveen LJ, Hoogeveen Y, Kool LJS, Renema WKJ, et al. Automatic segmentation of the wire frame of stent grafts from CT data. Med Image Anal. 2012 Jan 1;16(1):127–39.

49. Koenrades MA, Struijs EM, Klein A, Kuipers H, Reijnen MMPJ, Slump CH, et al. Quantitative Stent Graft Motion in ECG Gated CT by Image Registration and Segmentation: In Vitro Validation and Preliminary Clinical Results. Eur J Vasc Endovasc Surg. 2019 Nov 1;58(5):746–55.

50. Antoniou GA, Georgiadis GS, Antoniou SA, Kuhan G, Murray D. A meta-analysis of outcomes of endovascular abdominal aortic aneurysm repair in patients with hostile and friendly neck anatomy. J Vasc Surg. 2013 Feb 1;57(2):527–38.

51. Schuurmann RCL, Kropman R, Ouriel K, Jordan JWD, Muhs BE, Mannetje Y 't, et al. Remodeling of Abdominal Aortic Angulation and Curvature After Endovascular Aneurysm Repair in Patients With vs Without Late Type Ia Endoleak or Endograft Migration. J Endovasc Ther. 2021 Apr 4;28(2):342–51.

52. Diehm N, Katzen BT, Samuels S, Pena C, Powell A, Dick F. Sixty-four–detector CT Angiography of Infrarenal Aortic Neck Length and Angulation: Prospective Analysis of Interobserver Variability. J Vasc Interv Radiol. 2008 Sep 1;19(9):1283–8.

53. Diehm N, Kickuth R, Gahl B, Do D-D, Schmidli J, Rattunde H, et al. Intraobserver and interobserver variability of 64-row computed tomography abdominal aortic aneurysm neck measurements. J Vasc Surg. 2007 Feb 1;45(2):263–8.

54. Hendy K, Gunnarsson R, Cronin O, Golledge J. Infra-renal abdominal aortic calcification volume does not predict small abdominal aortic aneurysm growth. Atherosclerosis. 2015 Nov;243(1):334–8.

55. Schuurmann RCL, Overeem SP, van Noort K, de Vries BA, Slump CH, de Vries J-PPM. Validation of a New Methodology to Determine 3-Dimensional Endograft Apposition, Position, and Expansion in the Aortic Neck After Endovascular Aneurysm Repair. J Endovasc Ther Off J Int Soc Endovasc Spec. 2018 Jun;25(3):358–65.

56. de Rooy PM. Endograft position and apposition in aortoiliac seal zones and adaptive infrarenal neck enlargement after endovascular aneurysm repair [Master Thesis]. [Groningen]: University of Twente; 2020.

57. Chaikof EL, Blankensteijn JD, Harris PL, White GH, Zarins CK, Bernhard VM, et al. Reporting standards for endovascular aortic aneurysm repair. J Vasc Surg. 2002 May;35(5):1048–60.

58. Chaikof EL, Fillinger MF, Matsumura JS, Rutherford RB, White GH, Blankensteijn JD, et al. Identifying and grading factors that modify the outcome of endovascular aortic aneurysm repair. J Vasc Surg. 2002 May;35(5):1061–6.

59. Koo TK, Li MY. A Guideline of Selecting and Reporting Intraclass Correlation Coefficients for Reliability Research. J Chiropr Med. 2016 Jun;15(2):155–63.

60. van Noort K, Schuurmann RCL, Post Hospers G, van der Weijde E, Smeenk HG, Heijmen RH, et al. A New Methodology to Determine Apposition, Dilatation, and Position of Endografts in the Descending Thoracic Aorta After Thoracic Endovascular Aortic Repair. J Endovasc Ther. 2019 Oct 1;26(5):679–87.

61. Goudeketting SR, Schuurmann RCL, Slump CH, de Vries J-PPM. Changes in Apposition of Endograft Limbs in the Iliac Arteries After Endovascular Aneurysm Repair: Determination With New Computed Tomography–Applied Software. J Endovasc Ther. 2019 Dec 1;26(6):843–52.

62. Ghatwary T, Karthikesalingam A, Patterson B, Hinchliffe R, Morgan R, Loftus I, et al. St George's Vascular Institute Protocol: An Accurate and Reproducible Methodology to Enable Comprehensive Characterization of Infrarenal Abdominal Aortic Aneurysm Morphology in Clinical and Research Applications. J Endovasc Ther. 2012 Jun;19(3):400–14.

63. van Keulen JW, Moll FL, Tolenaar JL, Verhagen HJM, van Herwaarden JA. Validation of a new standardized method to measure proximal aneurysm neck angulation. J Vasc Surg. 2010 Apr;51(4):821–8.

64. Koenrades MA, Bosscher MRF, Ubbink JT, Slump CH, Geelkerken RH. Geometric Remodeling of the Perirenal Aortic Neck at and Adjacent to the Double Sealing Ring of the Anaconda Stent-Graft After Endovascular Aneurysm Repair. J Endovasc Ther. 2019 Dec;26(6):855–64.

65. Savlovskis J, Krievins D, de Vries J-PPM, Holden A, Kisis K, Gedins M, et al. Aortic neck enlargement after endovascular aneurysm repair using balloon-expandable versus self-expanding endografts. J Vasc Surg. 2015 Sep 1;62(3):541–9.

66. Kret MR, Tran K, Lee JT. Change in Aortic Neck Diameter after Endovascular Aortic Aneurysm Repair. Ann Vasc Surg. 2017 Aug 1;43:115–20.

67. Vukovic E, Czerny M, Beyersdorf F, Wolkewitz M, Berezowski M, Siepe M, et al. Abdominal aortic aneurysm neck remodeling after Anaconda stent graft implantation. J Vasc Surg. 2018 Nov 1;68(5):1354-1359.e2.

68. Guo J, Fujiyoshi A, Willcox B, Choo J, Vishnu A, Hisamatsu T, et al. Increased Aortic Calcification Is Associated With Arterial Stiffness Progression in Multiethnic Middle-Aged Men. Hypertension. 2017 Jan;69(1):102–8.

69. Lee K, Leci E, Forbes T, Dubois L, DeRose G, Power A. Endograft Conformability and Aortoiliac Tortuosity in Endovascular Abdominal Aortic Aneurysm Repair. J Endovasc Ther. 2014 Oct 1;21(5):728–34.

70. van Keulen JW, Moll FL, Barwegen GK, Vonken EPA, van Herwaarden JA. Pulsatile Distension of the Proximal Aneurysm Neck is Larger in Patients with Stent Graft Migration. Eur J Vasc Endovasc Surg. 2010 Sep 1;40(3):326–31.

71. Hazer D, Finol EA, Kostrzewa M, Kopaigorenko M, Richter G-M, Dillmann R. Computational biomechanics and experimental validation of vessel deformation based on 4D-CT imaging of the porcine aorta. In: Medical Imaging 2009: Biomedical Applications in Molecular, Structural, and Functional Imaging [Internet]. International Society for Optics and Photonics; 2009 [cited 2021 Jun 22]. p. 72621F. Available from: https://www.spiedigitallibrary.org/conference-proceedings-of-spie/7262/72621F/Computational-biomechanics-and-experimental-validation-of-vessel-deformation-based-on/10.1117/12.811765.short

72. Klein A, Oostveen LJ, Greuter MJW, Hoogeveen Y, Kool LJS, Slump CH, et al. Detectability of motions in AAA with ECG-gated CTA: A quantitative study. Med Phys. 2009;36(10):4616–24.

73. Schuurmann RCL, van Noort K, Overeem SP, Ouriel K, Jordan WD, Muhs BE, et al. Aortic Curvature Is a Predictor of Late Type Ia Endoleak and Migration After Endovascular Aneurysm Repair. J Endovasc Ther. 2017 Jun 1;24(3):411–7.

Appendices

Appendix A: Measurement protocol intra- and inter observer variability

Measurement session

Open new measurement

Open 3mensio. Drag the file of the patient you want to measure into the Local data of 3mensio. Go to the tab 'series' and select the scan with arterial contrast. If more scans are available select the scan with the most slices and the thinnest slices.

If you want to load all files from the external drive into 3mensio, go to 'options', archive and select the main file containing all patient files. Close 3mensio and open it again to load all patients. If that does not work press F5 to refresh.

Edit previous measurements

To edit a previous measurement, select the file of the patient you want to measure in the local data of 3mensio. Go to the tab 'sessions' and choose the saved session.

Segment Vessel

Make sure the following vessels are segmented by clicking on the aorta:

- Abdominal aorta,
- Common iliac arteries (left + right),
- External iliac arteries (left + right).

Use the slider to add or remove segmented parts. If arteries are missing they can be added with the 'add vessel' button. Use 'dimmed background' or 'segmentation only' view to check if all arteries of interest are segmented. If so, click 'confirm segmentation'.

Define Centerline

Aorta centerline

Draw the centerline by first clicking on the aortic lumen above the celiac trunk (+/- 5cm above the origin of the lowest renal artery) and second below the bifurcation in either one of the iliac vessels, this can be adjusted later. Click 'next'

Pre-EVAR: Move and add center points until the centerline is positioned in the center of the lumen. **Post-EVAR:** Move and add center points until the centerline is positioned in the center of the lumen of the main body of the Endograft, or the center between both legs of the endograft.

Switch to Snake View / Stretched Vessel for a good overview. Make sure the centerline runs from above the celiac trunk to below the aortic bifurcation (See figure 1). In bends a point should be placed before, after and in the middle of the curve.

Iliac centerline

Draw the centerline by first clicking on the aortic lumen above the truncus celiac trunk (+/- 5cm above the origin of the lowest renal artery), second above the aortic bifurcation and finally below both femoral bifurcations (right first) (See figure 2). Click 'next'. Move and add center points until the centerline is

positioned in the center of the lumen. In bends a point should be placed before, after and in the middle of the curve.

Figure 0-2 Aortic Centerline

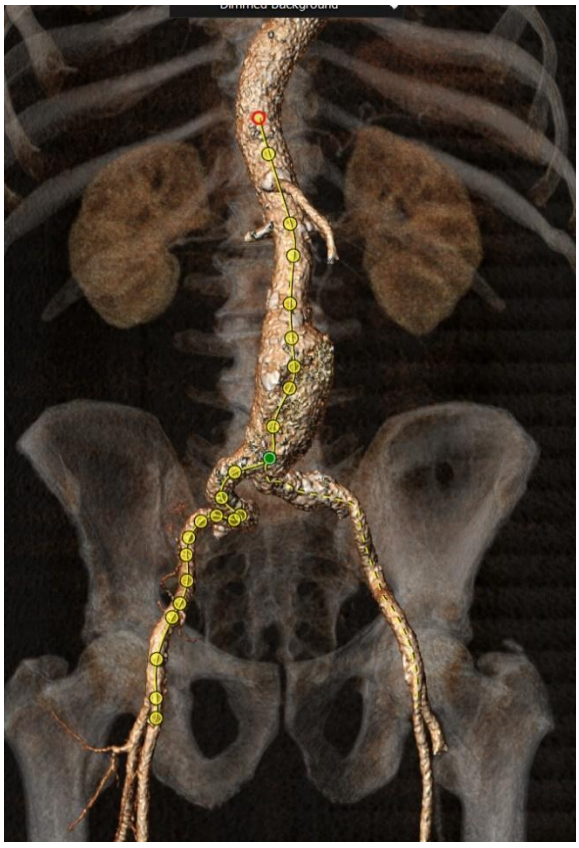

Figure 0-1 Iliac Centerline

Save session

Save the session with the study number and scan info. (Observer & Iliac/Aorta CLL)

Measurements

Aorta Centerline

Baseline

Navigate to the distal edge of the origin of the lowest renal artery and select 'Create baseline/ Move baseline here'. Make sure to indicate the prevalence of accessory renal arteries. Check on the postoperative scan where the endograft landing zone is located. If this is below the accessory renal artery then the distal edge of the origin of the accessory renal artery is the correct location for the baseline.

Thrombus/calcification

Pre-EVAR: Measure the maximum thrombus thickness of the neck on the perpendicular slice at -5 mm distance from the baseline, or at the slice where the most thrombus is visible in the neck. Note the amount of thrombus as percentage according to the Chaikof Criteria in REDCap:

- Absent; calcification <25% of circumference, atheroma, or thrombus (>2 mm thick) <25% of circumference;
- Mild; calcification 25% to 50% of circumference, atheroma, or thrombus (>2mm thick) 25% to 50% of circumference;
- Moderate; calcification 50% of circumference, atheroma, or thrombus (>2 mm thick) >50% of circumference.

The example in Figure 3 shows 0% thrombus/calcification.

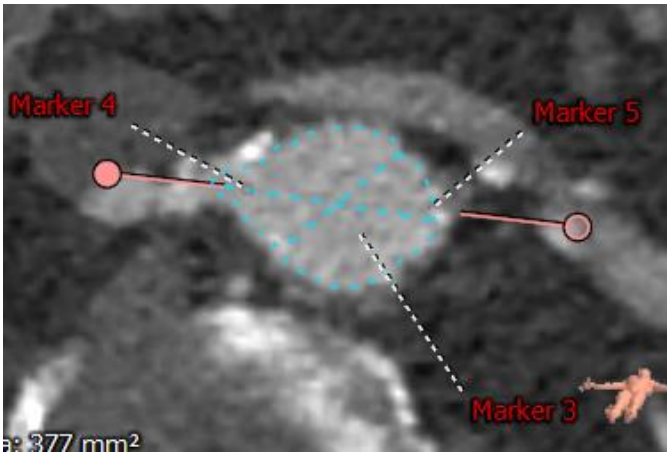

Figure 3 Example slice -5 mm from baseline

Markers

Place a marker in the perpendicular plane at the following locations:

- 1 at the distal edge of lowest renal artery orifice (baseline) (LRA)
- 1 at the distal edge of highest renal artery orifice (HRA)
- distal edge of truncus coeliacus (CTR)
- distal edge (SMA)
- 1 at the end of the neck (**pre-EVAR**) or end of circumferential apposition (**post-EVAR**) (See Neck/apposition length) (PEA)
- 1 at the aortic bifurcation (BIF)
- **Post-EVAR:** 1 at the proximal end endograft fabric (PF1)

Label the markers consistently in 3mensio! (See abbreviations above)

Neck Shape

Pre-EVAR: Define the neck shape (straight, conical, reversed conical, dumbbell) and note this in REDCap.

Neck diameter

Measure minimum and maximum diameter from adventitia to adventitia at the level of the baseline and at the level of the end of the neck. Note these in REDCap. If the wall is unclear, scroll through the perpendicular slices to follow the aortic wall.

Neck length

Pre-EVAR: Identify the first perpendicular slice distal to the lowest renal artery where the average diameter is increased with 10% compared to baseline. Measure the distance to the lowest renal artery (neck length). Note the length in REDCap. Do not use the 'neck measurement' option as this does not comply with the script that calculates the curvatures!

Alpha & Beta Angle

Pre-EVAR: Use the tool centerline angle in 3mensio. Alpha angle (degrees): The maximum angle between the luminal axis of the suprarenal aorta and the infrarenal neck. Beta angle (degrees): maximum angle between the luminal axis of the infrarenal neck and the aneurysmal sac. Note these in REDCap.

Maximum aneurysm diameter

Pre-EVAR: Scroll through the aneurysm to find the location of the maximum diameter (incl. thrombus). Measure at this location the maximum and minimum diameter from adventitia to adventitia. Note these in REDCap.

Save & Export session (required by VIA software)

Prior to exporting the measurement sessions an empty folder should be created on the external drive. Give the folder the name "StudyID"_"ScanID", for example D1001_Pre of D1001_FU1.

After saving and closing the measurement session in 3mensio, select the session in the 'sessions' tab, and export the measurement file to the study folder using right mouse button and select 'export to folder'. Select the correct folder.

Iliac Centerline

Markers

Place a marker in the perpendicular plane at the following locations:

- **Post-EVAR** End of endograft right (DRF1)
- **Post-EVAR** End of endograft left (DLF1)
- proximal edge of origin of internal iliac artery right (RII)
- proximal edge of origin of internal iliac artery left (LII)
- proximal edge of the origin of the femoral profunda artery right (RFP)
- proximal edge of the origin of the femoral profunda artery left (LFP)

Label the markers consistently in 3mensio. See abbreviations above

Iliac Aneurysm

Pre-EVAR: Mark in REDCap if an aneurysm in the common iliac artery is present. The presence of a common iliac artery aneurysm (CIAA) is defined as a CIA diameter ≥25 mm in an isolated region or along the whole CIA.

Save & Export session (required by VIA software)

Prior to exporting the measurement sessions an empty folder should be created on the external drive. Give the folder the name "StudyID"_"ScanID", for example D1001_Pre of D1001_FU1.

After saving and closing the measurement session in 3mensio, select the session in the 'sessions' tab, and export the measurement file to the study folder using right mouse button and select 'export to folder'. Select the correct folder.

Note: In the newest version of 3mensio the CLLs are not automatically exported. The CLL should therefore be exported separately. Open the measurement session and chose the 'advanced' tab in the right panel. Chose 'Export Segmentation Results' and save the text-file using the same names as defined for the folder.

Dankwoord (in Dutch)

Deze thesis is de afsluiting van mijn opleiding technische geneeskunde. Ik heb de afgelopen jaren niet alleen veel geleerd op technisch en medisch gebied, maar ik heb mijzelf ook mogen ontwikkelen tot jonge professional op persoonlijk vlak. Met name tijdens mijn afstuderen heb ik hier veel aan kunnen werken. Ik kijk terug op een erg fijne tijd in het MST, ik heb mij hier als een vis in het water gevoeld. Ik wil daarom graag de heelkunde afdeling van het MST bedanken voor de leuke en leerzame stage. Ik heb hier veel verschillende mensen mogen ontmoeten van wie ik veel heb kunnen leren. In het bijzonder wil ik mijn medisch begeleider en voorzitter van mijn afstudeercommissie dr. Bob Geelkerken bedanken. Bedankt voor het vertrouwen in mijn kunnen en bovenal voor het creëren van een omgeving waarin ik ook heb leren vertrouwen op mijn eigen kunnen. Bovendien wil ik Jaimy bedanken voor alle dagelijkse begeleiding, vaak onder het genot van een lekkere koffie. Ik wens iedere andere TGer een begeleider zoals jij toe. Een begeleider die tijd voor je maakt, altijd klaar staat met goede adviezen of tips en ook zeker ruimte over laat voor gezelligheid. Samen hebben we ups en de downs meegemaakt van het onderzoek doen.

Ook wil ik mijn begeleiding vanuit het UMCG bedanken. Richte en dr. Jan-Paul de Vries bedankt voor jullie begeleiding en discussies die mij nieuwe stof tot nadenken gaven. Daarnaast wil ik ook Roy, Claire en Marjolein bedanken die mij iedere keer hebben geholpen aan een online verbinding met het UMCG.

Ik wil natuurlijk ook mijn begeleiders op de UT bedanken. Prof. Kees Slump, bedankt voor de begeleiding en de goede adviezen. Geweldig dat deze adviezen ook per mail paraat staan op donderdag avonden wanneer een experiment in Arnhem dreigt te mislukken. Ruby, bedankt voor je fijne proces begeleiding. Ik was eerst niet blij dat ik halverwege mijn afstuderen een andere procesbegeleider kreeg, maar die mening heb ik direct bijgesteld na onze eerste ontmoeting. Ik heb onze intervisiegesprekken erg waardevol gevonden en ben blij dat ik je nog een halfjaar heb mogen leren kennen. Daarnaast wil ik nog de mensen uit de vakgroep M3i bedanken voor de leuke en waardevolle gesprekken en de hulpvaardigheid bij mijn problemen. Ook wil ik Michelle Heijblom bedanken voor het bekleden van de rol als mijn buitenlid.

Dan wil ik nog graag een aantal mensen bedanken die veel hebben betekend voor het 8 vs 10 fasen onderzoek. Gerben en Henny, bedankt voor het in elkaar knutselen en samen testen van mijn gebruikte opstelling. Jullie vindingrijkheid werd enorm gewaardeerd en ik heb ook veel van jullie kunnen leren. Frank, bedankt dat je ons steeds weer wilde ontvangen in Arnhem voor het opnieuw maken van de CTs. Majorie & Daphne, bedankt voor de tijd die jullie hebben gestopt in het steeds toezenden van alle data.

Mijn studenten tijd was natuurlijk niet compleet zonder mijn lieve studievriendinnen Annabel, Anne, Denise, Lianne, Maritta, Marjolein, Nynke en Tess. Bedankt dat ik altijd op jullie kan rekenen!

Als laatst wil ik mijn familie bedanken. Lieve pap en mam, Talitha, Naomi, Jesse en Silas bedankt voor al jullie lieve zorgen en steun, ondanks dat ik tijdens mijn studie op kamers ben gegaan voelt Vroomshoop nog als mijn veilige thuishaven en hoop ik snel weer terug te verhuizen. Uiteraard samen met mijn lieve Joshua. Bedankt voor het aanhoren van mijn stress en mijn klagen, bedankt dat je toch altijd positief bleef en mij de zonnige kanten kon laten zien waardoor ik weer kon lachen. Orlando, bedankt voor je creatieve bijdrage!

Oja, dan wil ik ook nog Siepie en Lotje bedanken voor het actief participeren in bijna al mijn online meetings. Ik denk dat bovenstaande namen dit allen kunnen beamen.

Ik wens jullie allen het beste,

Deborah

Een lachend gezicht verblijdt het hart

Een goed bericht verkwikt het lichaam

Wie luistert naar de lessen van het leven schaart zich onder de wijzen

Wie zich niet laat terechtwijzen doet zichzelf tekort

Wie berispingen ter harte neemt , wint daarbij

Wie ontzag heeft voor de Heer wint aan wijsheid

Spreuken 15:13 e,v.